Tectonics

RESEARCH ARTICLE
10.1029/2020TC006227

Key Points:

- Structural and geoelectrical data provide an image of the volcano-tectonic structure characterizing the Pisciarelli fumarole field
- The fault system in the Solfatara-Pisciarelli area acts as the main conduit for hydrothermal fluids in the caldera
- A possible volcanic hazard scenario for this caldera sector, linked to morphological and hydrothermal evolution, is suggested

Correspondence to:
R. Isaia,
roberto.isaia@ingv.it

Citation:
Isaia, R., Di Giuseppe, M. G., Natale, J., Tramparulo, F. D. A., Troiano, A., & Vitale, S. (2021). Volcano-tectonic setting of the Pisciarelli fumarole field, Campi Flegrei caldera, southern Italy: Insights into fluid circulation patterns and hazard scenarios. *Tectonics*, *40*, e2020TC006227. https://doi.org/10.1029/2020TC006227

Received 7 APR 2020
Accepted 21 APR 2021

Volcano-Tectonic Setting of the Pisciarelli Fumarole Field, Campi Flegrei Caldera, Southern Italy: Insights Into Fluid Circulation Patterns and Hazard Scenarios

Roberto Isaia[1], Maria Giulia Di Giuseppe[1], Jacopo Natale[2], Francesco D'Assisi Tramparulo[1], Antonio Troiano[1], and Stefano Vitale[1,2]

[1]Istituto Nazionale di Geofisica e Vulcanologia, Sezione di Napoli Osservatorio Vesuviano, Napoli, Italy, [2]Dipartimento di Scienze della Terra, dell'Ambiente e delle Risorse (DiSTAR), Università degli Studi di Napoli Federico II, Napoli, Italy

Abstract Phreatic and hydrothermal eruptions are small energetic explosive events that generally have few to no precursors and represent a considerable hazard in tourist and urban areas. At the Campi Flegrei caldera, these events have occurred at the Solfatara volcano and have likely occurred at the nearby Pisciarelli site, where the most powerful hydrothermal phenomena are located. Here, increased hydrothermal activity has caused relevant morphological changes that has led local authorities to deny access to the site. Stratigraphic, structural, and geophysical investigations have allowed us to reconstruct the volcano-tectonic setting of the area. In particular, we have recognized a fault system and related damage zones that act as the preferred pathway for hydrothermal fluids in the caldera. At the surface, these faults control the migration and/or accumulation of deep-seated gases into the subsoil and the formation of fumaroles and mud pools. We have recognized two main fault systems with different ages that show variable displacements. The electrical anomalies identified by electrical resistivity tomography further highlight the main fault pattern and show the interplay between volcano-tectonic structures and fluid circulation. Host rocks and fault zones may be involved in self-sealing processes and/or rock failure phenomena capable of modifying the fluid pathways and establishing favorable conditions, leading to overpressure and/or rapid decompression of fluids and triggering an explosive event. Furthermore, stratigraphic mapping shows fossil mud pool sediments embedded in an old debris flow located above the modern hydrothermal system. This implies that they were at a higher elevation when they formed. The morphotectonic evolution and intense rock alterations in the area could promote further landslide episodes, producing debris-flow deposits that can cover the active area and possibly trigger hydrothermal/phreatic events.

1. Introduction

Active calderas are complex volcanic systems that typically host hydrothermal manifestations such as fumaroles, mud pools, and steaming grounds (e.g., Mayer, Scheu, Yilmaz, et al., 2017; Montanaro, Mayer, et al., 2017; Montanaro, Scheu, et al., 2016; Morgan et al., 2009). The location and intensity of these phenomena provide insights into the volcanic activity state, and their temporal variations help to unravel the possible evolution of the hosting volcanic system. Fumarolic and hydrothermal activities are generally localized within the crater area and along the volcano rim and flanks. Furthermore, they can also be focused along former eruptive fissures and local to regional faults and their damage zones (Geshi et al., 2016; Heap, Lavallée, et al., 2014; Kobayashi & Hatano, 1989; Seki et al., 2015). These fractured rocky bodies may be the preferential paths for the migration of magmatic and hydrothermal fluids and may potentially represent conduits for phreatic and hydrothermal explosions (Gallagher et al., 2020; Montanaro, Cronin, et al., 2020). Volcanoes hosting active fumarolic and hydrothermal fields, where such kinds of events recently occur, are numerous worldwide (e.g., Ruapehu, New Zealand; Boiling Lake, Dominica; Hakone, Japan; and Telica, Nicaragua). Hydrothermal fields are locations of occasional phreatic eruptions, which are often preceded by sudden and/or cryptic precursory signals (e.g., Dempsey et al., 2020; Harada et al., 2018; Hurst et al., 2014; Ohba et al., 2019; Roman, Rodgers, et al., 2016; Salvage et al., 2018) and in some cases, cause many fatalities (e.g., Whakaari-White Island, New Zealand; Ontake, Japan) (e.g., Edwards et al., 2017; Hanagan et al., 2020; Hurwitz et al., 2016; Kilgour et al., 2019; Mannen et al., 2018; Roman, LaFemina, et al., 2019; Rott et al., 2019). The processes that trigger these events are different from system to system, and their

identification is challenging (e.g., Geshi et al., 2016; A. Jolly et al., 2018; Mayer, Scheu, Yilmaz, et al., 2017; Rott et al., 2019; Stix & de Moor 2018). The main mechanisms include the rapid decompression of the hydrothermal system, likely caused by rock failure associated with earthquakes and landslide phenomena (A. D. Jolly et al., 2014) or sudden hydrological variations (Gallagher et al., 2020). Another cause may be a renewed magma intrusion that determines a critical overpressure within the system with a magmatic fluid injection and flashing of the hydrothermal reservoir (e.g., de Moor et al., 2016; Gallagher et al., 2020; Geshi et al., 2016; Mayer, Scheu, Montanaro, et al., 2016; Mayer, Scheu, Yilmaz, et al., 2017; Montanaro, Cronin, et al., 2020; Rott et al., 2019). The self-sealing process also has to be considered among the trigger mechanisms (Gallagher et al., 2020; Heap, Gravley, et al., 2020; Kennedy et al., 2020; Roman, LaFemina, et al., 2019). It consists of fractures and pores being sealed through mineralizations (Geirsson et al., 2014; Roman, Rodgers, et al., 2016; Tajima et al., 2020), leading to reduced rock permeability and a rise in fluid pressure (Christenson, Reyes, et al, 2010; Christenson, White, et al., 2017). Furthermore, landslides can also cause phreatic explosions by covering and sealing the gas emission zones, fumarole vents, or mud pools, as described by Rott et al. (2019).

Frequently, phreatic eruptions are generated at very shallow volcanic levels and consist of short-lived and impulsive explosions (Gallagher et al., 2020; Montanaro, Cronin, et al., 2020), spreading a mixture of acidic gases and hot pyroclastic materials on areas reaching square kilometers around the vent; this has been reconstructed, for instance, for Solfatara eruptive activity (Isaia, Vitale, Di Giuseppe, et al., 2015). It follows that the study of phreatic eruptions is mandatory for defining volcanic hazards. With this aim, crucial geological features need to be assessed. They include (1) the characterization of the main structures that determine the rise of liquids and gases in the emission zones, (2) their interconnection, which favors gas accumulation or leakage, and (3) the possible interactions of these structures with shallow water reservoirs and the hydrothermal system. All these elements, together with the geological and physical characterization of the host rocks and the geochemical definition of fluids, contribute to a full description of the volcano-tectonic framework of the fumarolic-hydrothermal emission areas. The description of these features also aids in the understanding of the evolution and the possible abrupt change within the volcanic system. Furthermore, the reconstruction of the structural architecture of these active sectors is fundamental for interpreting geochemical and deformation monitoring data and the development and management of the monitoring networks themselves.

With this in mind, we performed multidisciplinary investigations to define the structural setting of the Pisciarelli fumarolic-hydrothermal area located on the outer eastern flank of the Solfatara volcano within the Campi Flegrei caldera (Figure 1). This caldera sector hosts several fumarole vents, thermal springs, and boiling mud pools, both within the Solfatara crater and along its flanks. Furthermore, this area is characterized by a dense network of fractures and faults, which has allowed the emplacement of lava domes and the formation of an extensive hydrothermal system involved in phreatic and small hydrothermal explosions (Isaia, Vitale, Di Giuseppe, et al., 2015; Montanaro, Mayer, et al., 2017). Over the last few years, the Pisciarelli site has been characterized by significant morphological variations in the emission zone, geochemical characteristics of the fluids, and some mud emission episodes (INGV, 2020; Tamburello et al., 2019). In this study, we produced detailed volcanological and structural maps through stratigraphic and structural surveys. We performed geophysical investigations to characterize the fumarolic field structure consisting of electrical resistivity tomography (ERT) surveys. This technique allows for imaging and reconstruction of the shallow, subsoil fluid distribution, down to a depth of approximately 100 m. Furthermore, by identifying faults on the surface and their continuation at depth through the study of electrical resistivity anomaly patterns, some hypotheses on the interplay between volcano-tectonic structures and hydrothermal activity have been proposed. Structural and geophysical results may help to evaluate the present state of this active area, which is presently considered among the most hazardous within the Campi Flegrei caldera, particularly for the possible occurrence of phreatic/hydrothermal explosions (e.g., Isaia, Vitale, Di Giuseppe, et al., 2015).

10.1029/2020TC006227

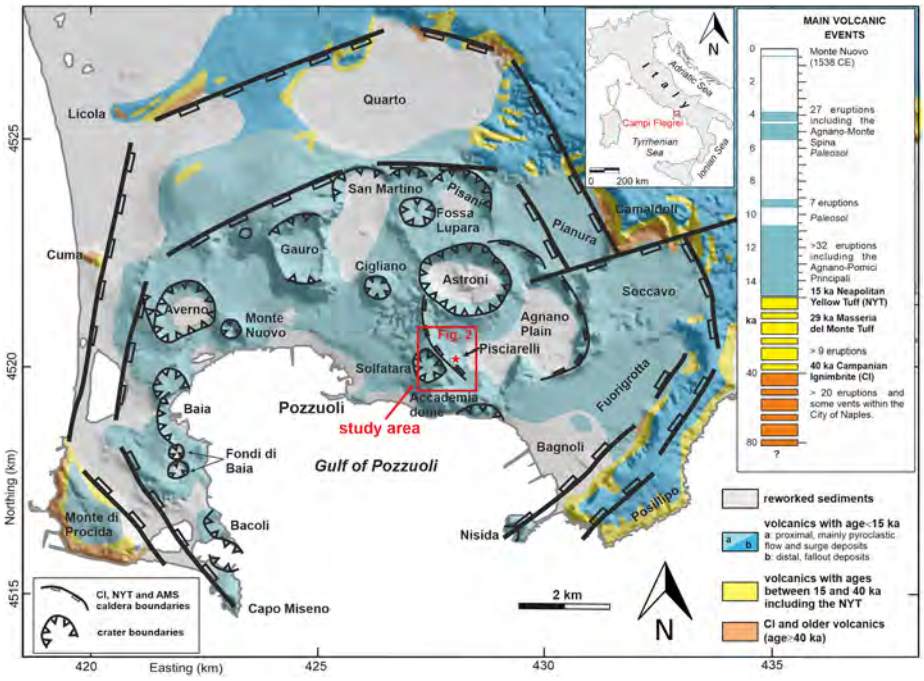

Figure 1. Simplified geologic map of the Campi Flegrei caldera (modified after Vitale et al., 2019). (UTM projection, Zone 33, Datum WGS84, km).

2. Geological Setting of the Campi Flegrei Caldera

The volcanic field of the Campi Flegrei caldera has experienced volcanism since at least 80 ka. Following the Campanian Ignimbrite (CI) eruption, its structure was profoundly changed (40 ka; Giaccio et al., 2017) with the formation of a 12 km diameter caldera, and later, with some significant events, among which the most energetic was the Neapolitan Yellow Tuff (NYT) eruption (15 ka; Deino et al., 2004). These events produced a nested caldera characterized by tangential and concentric ring faults with dominant normal kinematics (Vitale & Isaia, 2014). In the last 15 ka, the NYT caldera has been the site for at least 70 eruptive episodes (Bevilacqua, Isaia, et al., 2015; Di Vito, Isaia, et al., 1999; Isaia, Marianelli, & Sbrana, 2009; Orsi et al., 2004; Smith et al., 2011). In that period, volcanic activity was mainly focused in the central-eastern sector of the caldera, which is presently considered the area that is most prone to local new vents, in a possible resumption of volcanism (Bevilacqua, Flandoli, et al., 2016; Bevilacqua, Isaia, et al., 2015; Bevilacqua, Neri, Bisson, et al., 2017; Orsi et al., 2004; Rivalta et al., 2019; Selva et al., 2012; Vilardo et al., 2010), and has recorded different phreatic events (Isaia, Vitale, Di Giuseppe, et al., 2015). The most recent volcanism (4.3–3.5 ka; Epoch 3B; Smith et al., 2011) has occurred along the western border of the Agnano Plain (Figure 1), which in turn resulted from the formation of a minor caldera following the Plinian Agnano-Monte Spina eruption (4.55 ka; de Vita et al., 1999; Smith et al., 2011). The Agnano Plain is an approximately 3 km in diameter depressed area (Figure 1) surrounded by a segmented rim bounded by ring faults. In general, the caldera central sector hosts several high-angle faults associated with the last volcano-tectonic activity that frequently reactivated preexisting deep-seated faults (e.g., Vitale et al., 2019). Epoch 3B includes a cluster of small volcanic edifices within and around the present Solfatara maar-diatreme volcano (Isaia, Marianelli, & Sbrana, et al., 2009; Isaia, Vitale, Di Giuseppe, et al., 2015), which erupted contemporaneously with the Averno volcano located in the western caldera sector (Pistolesi et al., 2016). Two large volcanoes (Astroni and Fossa Lupara; Figure 1), located along a NW-SE trending fissure a few km northward of the Solfatara crater, formed immediately after the Solfatara eruption (Di Vito, Isaia, et al., 1999; Isaia, D'Antonio, et al., 2004; Isaia, Marianelli, & Sbrana, 2009). Finally, the last historical eruption occurred in 1538 CE, forming the Monte Nuovo cone (Figure 1; Di Vito, Lirer, et al., 1987; Guidoboni & Ciuccarelli, 2011).

In the last 15 kyr, Campi Flegrei experienced alternating uplift and subsidence episodes, which mainly affected its central sector. Generally, the uplift of the ground, reaching several tens of meters, was accompanied

by seismovolcanic events that were frequently coupled with volcanism (e.g., Isaia, Vitale, Marturano, et al., 2019; Marturano et al., 2018; Vitale et al., 2019). A ground uplift of approximately 15 m preceded the Monte Nuovo eruption (Di Vito, Acocella, et al., 2016), and ground movements (called bradyseism) on the order of 1–10 m have been detected since Roman times (more than 2,000 years ago; e.g., Bellucci et al., 2006; Parascandola, 1947) and have continued to the present (Del Gaudio et al., 2010; INGV, 2020). Recent structural studies in the Campi Flegrei caldera, both inland (Isaia, Vitale, Di Giuseppe, et al., 2015; Vitale & Isaia, 2014; Vitale et al., 2019) and offshore (e.g., Natale et al., 2020), have shown that faults are located close to volcanic vents and caldera rims. These structures are associated with both eruptive and ground deformation activity (e.g., Bevilacqua, Neri, De Martino, et al., 2020). Generally, these structures show a prevalence of regional tectonic directions (NW-SE and NE-SW); however, NNE-SSW- and WNW-ESE trending faults are associated with the youngest deformational episodes within the caldera (e.g., Vitale & Isaia, 2014; Vitale et al., 2019). According to Vitale and Isaia (2014), the fault orientation is the result of the interplay between the regional tectonic field associated with the opening of the Tyrrhenian Sea (Vitale & Ciarcia, 2013) and the local volcano-tectonic deformation. The central sector is also characterized by intense degassing and hydrothermal activity (e.g., Cardellini et al., 2017; Chiodini, Caliro, et al., 2012) and by the highest values of surface fractures and fault density, particularly around the town of Pozzuoli and in the Solfatara area (Bevilacqua, Isaia, et al., 2015; Bevilacqua, Neri, De Martino, et al., 2020).

3. Volcano-Tectonic Setting of the Pisciarelli Fumarole Field

The Pisciarelli area is located on the eastern margin of the structural high between the Solfatara maar and the Agnano Plain (Figure 2). The main fumaroles and mud pool (Figures 3a–3e) occur along the intersection of the NW-SE-trending ring faults of the Agnano caldera and the major ENE-WSW fault passing through the Solfatara crater (Figure 2a). Other fumaroles, with temperatures reaching 100°C, are present, both southward (in Antiniana) and northward (in the old alum quarry) of the Pisciarelli site. These fumarolic centers are evident in CO_2 emission maps (Cardellini et al., 2017). The Pisciarelli fumarole field has recently experienced relevant changes in the CO_2 flux (of a maximum of 600 tons/d, Tamburello et al., 2019), geochemical indicators, and the morphology of the main emission zone. In the Pisciarelli area, since 2005, the CO_2 flux has increased with the formation of a well-defined main fumarole (Figures 3a–3c), with an average temperature of 115°C (INGV, 2020) and an increasingly extensive and active mud pool characterized by different gas emission boiling points (Figures 3a and 3c–3e). More recently, the degassing phenomena has created a large crackling mud bubble area (Figure 3d), which significantly changes seasonally. Morphological changes involve both the eastern flank of the Solfatara volcano (Figures 4a–4f) and the fumarole and mud pool areas (Figures 4g–4i). The slope is characterized by an active landslide that has produced several debris flow deposits (Figure 3f), where large boulders have also been mobilized. Figures 4a–4g shows aerial photographs of the analyzed area from 1929 to 2020. The landslide area was already active between 1929-1943 (Figures 4a and 4b), and in 1998 (Figure 4c), intense urbanization of the area is evident. By comparing the satellite images of the head scarp in 2007 and 2019 (Figures 4d and 4e), a receding slope is evident, creating a cutting slope in the upper part. Finally, satellite images (Figures 4f and 4g) show the formation of several minor head scarps and an unstable rock mass located to the right of the main landslide (inset of Figure 4f). The recent image of the Pisciarelli fumarole field (Figure 4g) shows the mud pool with a maximum length of ca. 15 m, resulting from an enlargement mainly to the W-NW of the original water boiling point in the last 15 years. From July to September 2020, the pool level experienced a sharp drop of approximately 3 m (Figures 4h and 4i), which was accompanied by small mud spatters around the pool (Figures 4h and 4i). After this episode, a recharge period coincided with meteoric water input, which brought the mud pool level back to the previous and present levels.

3.1. Stratigraphy

To better define the stratigraphic and structural setting, we performed a geological survey of the area and produced the geological map shown in Figures 2a and 5. The study area is characterized by diffuse hydrothermal manifestations that affect the exposed rocks with severe alteration. These rocks were emplaced during the most recent activity (in the last 5.5 kyr) of the central sector of the caldera (Figures 2a and 2c). The oldest exposed deposits are from vents located in the present Agnano Plain, with ages ranging between

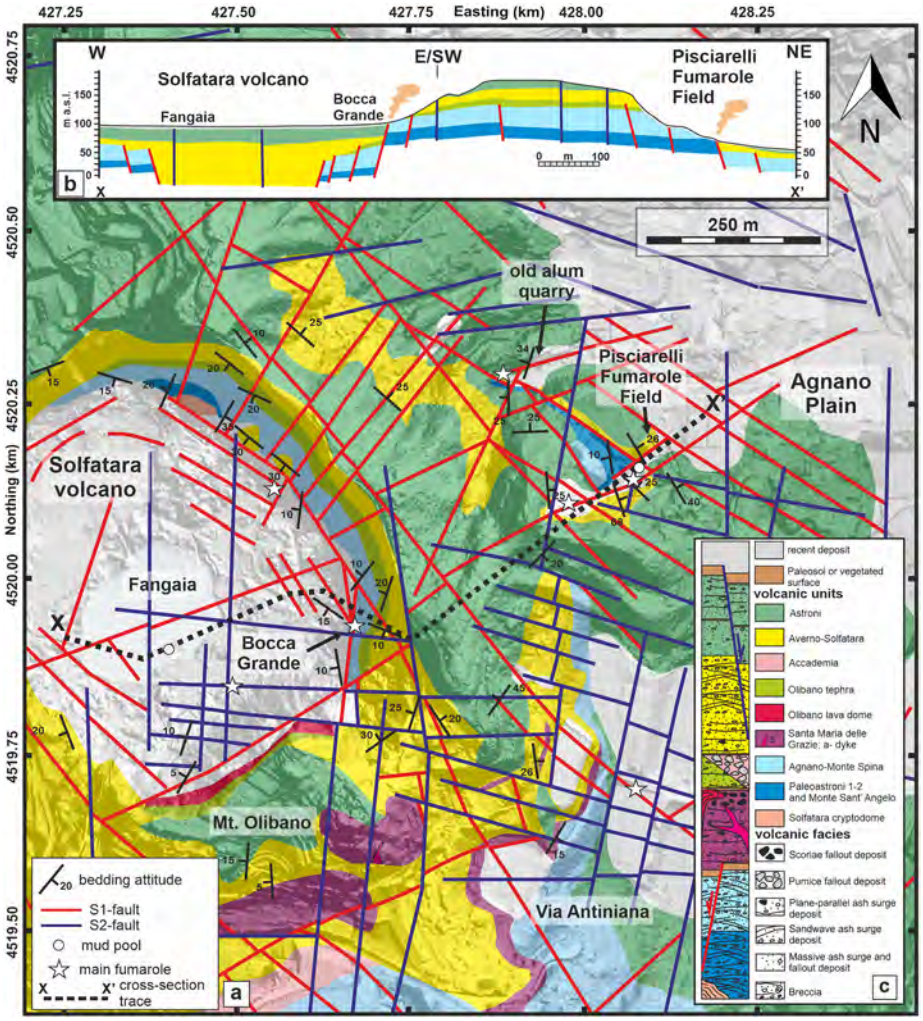

Figure 2. (a) Geologic map of the Solfatara-Pisciarelli area, from this study. (UTM projection, Zone 33, Datum WGS84, m). (b) Geologic cross-section (modified after Isaia, Vitale, Di Giuseppe, et al., 2015). (c) Schematic stratigraphic log.

4.9 and 4.55 ka (Smith et al., 2011). They are overlain by younger deposits of Solfatara and Astroni eruptions (4.28–4.25 ka). The oldest rocks show beds gently dipping toward the west, while the younger deposits unconformably overly this sequence, following the resulting paleomorphology after the Agnano-Monte Spina caldera collapse. The rocks are mainly composed of alternating coarse and fine pyroclastic materials and are often profoundly altered by secondary mineralization due to fumarolic and hydrothermal activity. Alteration processes have changed the mechanical properties of the rocks, favoring the lithification of loose sediments (Kennedy et al., 2020; Mayer, Scheu, Montanaro, et al., 2016). The physicochemical variation in the rocks makes it difficult to attribute and correlate to well-known eruptions. Nonetheless, the paleosols are well-preserved, favoring deposit recognition. The stratigraphy of the area is defined by the superposition of several volcanic deposits (Figure 2c; Isaia, Vitale, Di Giuseppe, et al., 2015; Vitale et al., 2019), including, from bottom to top, the Monte Sant'Angelo (MSA, ~4.92 ka), Paleoastroni 2 (PA2, ~4.73 ka), Agnano-Monte Spina (AMS, ~4.55 ka), Santa Maria delle Grazie (SMG), Olibano tephra (OLI), Solfatara (AVS, ~4.28 ka), and Astroni (AST, ~4.25 ka) deposits. The oldest volcanic deposits (MSA and PA2), hereafter referred to as pre-AMS, are exposed in the Pisciarelli fumarole field along a NW-SE direction and are bounded by NW-SE major faults and covered directly and unconformably by AVS deposits (Figure 6a). South of the Pisciarelli fumarole field, pre-AMS deposits are covered by AMS pyroclastics, which are in turn overlain by scoria in the SMG and OLI deposits and pyroclastic rocks of the AVS and AST deposits (Figure 6b). The passage to the AVS deposit is marked by a muddy layer with leaves and charcoal fragments. The area is highly altered

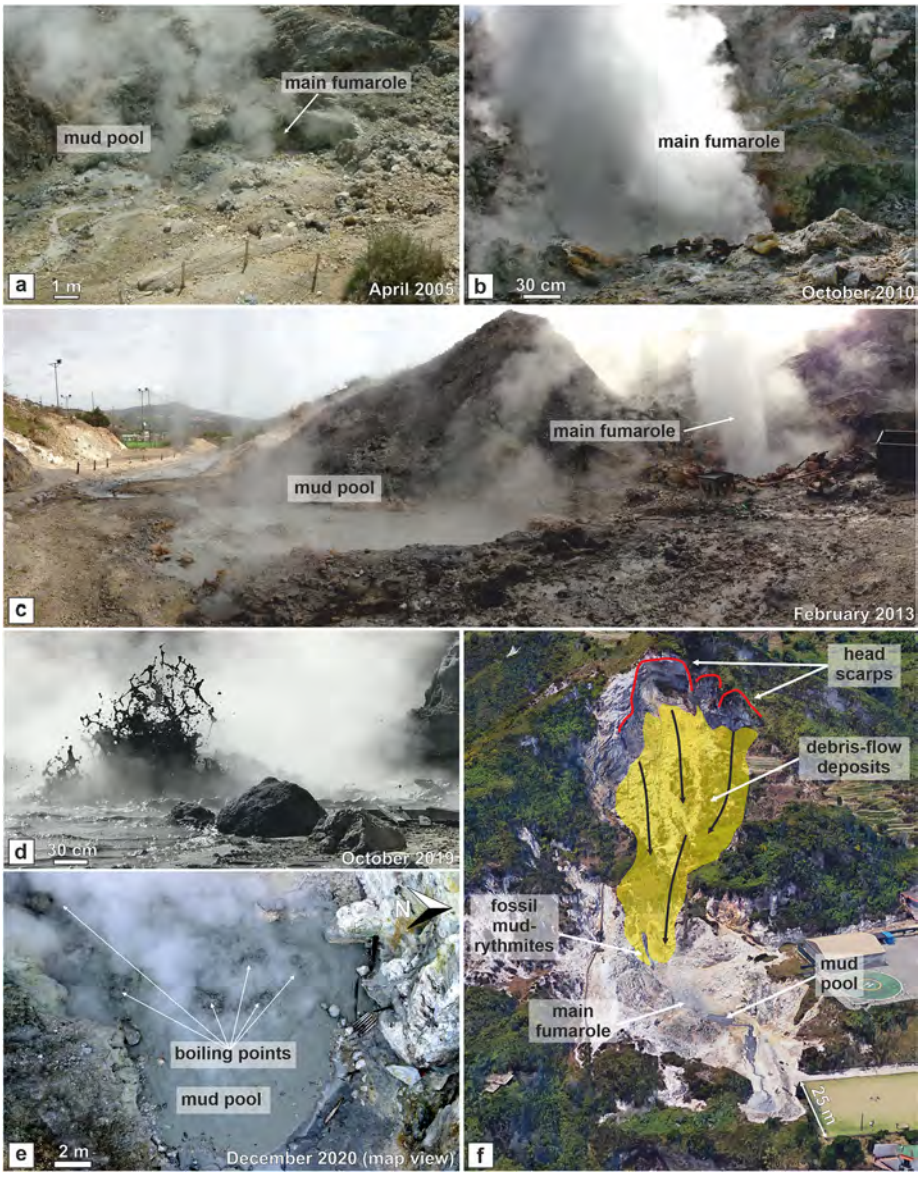

Figure 3. (a–e) Pictures show fumarole and mud pool activity from 2005 up to 2020. Picture (e) was obtained by Unmanned Aerial Vehicle (UAV). (f) Google Earth 3D image (2019) of the Pisciarelli fumaroles field showing the line drawing of the debris flow deposits and head scarps.

by hydrothermal activity, and in some localities, the alteration has affected only part of the succession (Figure 7a). Different paleosols are present; among others, the most developed paleosol occurs on top of the AMS deposit. Close to the main fumarole and mud pool, the volcanic succession is covered by several debris flow clastic deposits (named DF1-4 in Figures 6b and 6c) that are locally well cemented (Figure 6f) and embed a sedimentary sequence of mud rhythmites (Figures 6c–6e), which are located ca. 14 m above the current mud pool.

3.2. Deformation Structures

Fractures and faults highly deform the whole volcanic sequence in the Pisciarelli area. Syn-sedimentary deformation structures are high-angle fractures and low-to high-angle normal faults (named system S0), which are especially hosted in the AVS deposits. They include faults with associated drag folds and growth strata (Figure 6g). In particular, where the beds show moderate to steep dips, high-angle fractures and

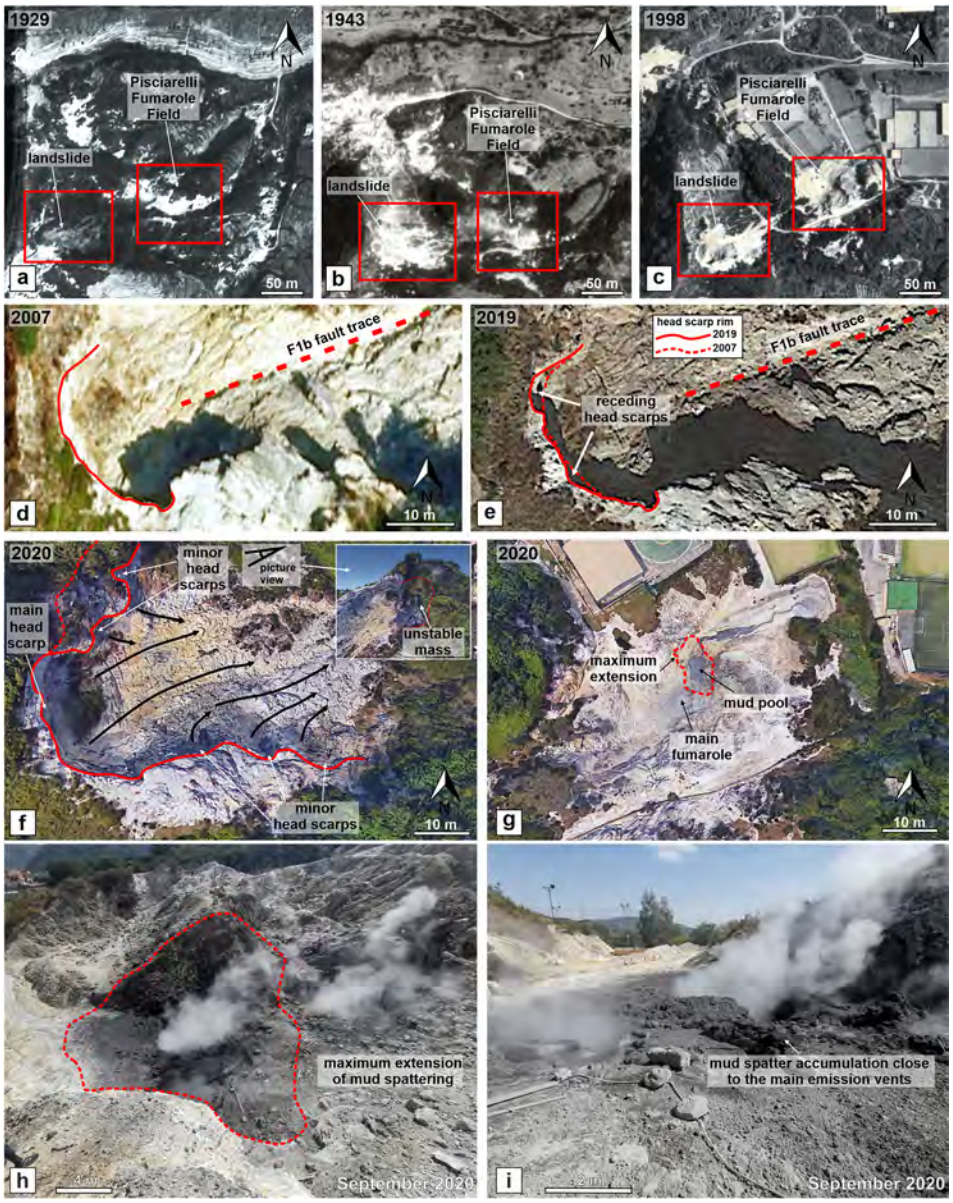

Figure 4. (a–c) Aerial photographs of the Pisciarelli area in 1929, 1943, and 1998. (d–g) Satellite images at 2019–2020 (from Google Earth). (h) Pisciarelli dried mud pool with indicated area covered by mud spatters. (i) Mud spatter accumulation close to the dried mud pool in September 2020.

small-scale normal faults pervasively affect the rocks (Figure 6a). At larger scale the whole area is affected by two fault systems (S1 and S2), which are both characterized by two mutually orthogonal sets. Kinematic indicators are rarely present. However, a dominant normal dip-slip with a secondary oblique-slip movement for all faults is observed, which is consistent with what has been reported in the whole Campi Flegrei caldera (Vitale & Isaia, 2014). This feature is further supported by the evidence that several faults appear as conjugate structures with a subhorizontal intersection, suggesting dominant dip-slip kinematics. We have recognized the first system of volcano-tectonic faults (S1) as structures crosscutting the pre-AMS and AMS deposits and covered by the AVS tephra (Figures 6a, 6b, 6h, 7a, and 7b). Generally, these faults show a well-preserved fault scarp with the AVS deposit mantling it, often showing high dip values (60°–90°) (Figures 6a, 6h, 7a, and 7b). These major faults are defined by a dominant NW-SE strike generally dipping to the NE and a secondary NE-SW direction, which both usually show displacements of a few tens of meters. Within the S1 system, we have identified two principal faults, named F1a and F1b; at their intersection, the

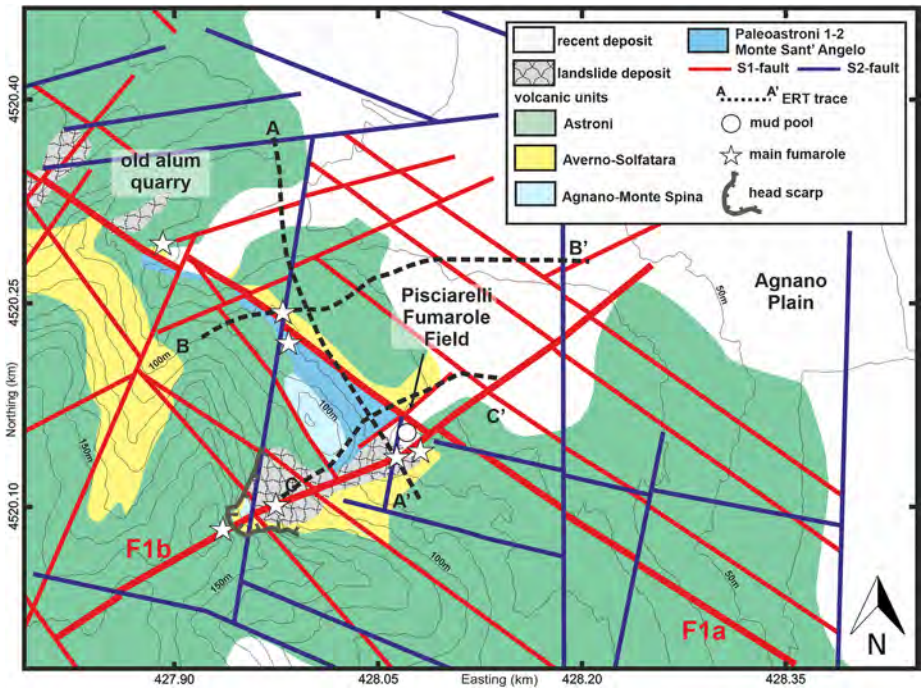

Figure 5. Detail of the geologic map of the Pisciarelli area, including the location of main fumaroles and mud pool; main faults named F1a and F1b are also highlighted. (UTM projection, Zone 33, Datum WGS84, m).

mud pool area is located. The second fault system (S2) typically consists of E-W/ESE-WNW- and NNE-SSW-trending planes that cut the S1 faults and the AVS and AST deposits (Figure 7c). The dip angles for this fault system range from 70° to 90°, and the maximum displacements are a few meters. A synsedimentary NNE-SSW-trending S2 fault bounds the eastern side of mud rhythmites with a displacement of a few centimeters (Figure 6d). The structural study of mesoscale faults and fractures has provided ~100 fault data points and ~700 fracture data points. Poles to fault planes and corresponding rose diagrams mark the occurrence of two main directions well (Figure 8): NW-SE for S1 (Figure 8a) and E-W for S2 (Figure 8b). On the other hand, fractures show a prevailing WNW-ESE direction (Figure 8c).

4. Resistivity Survey

Geophysical investigations are very useful to reconstruct the structural pattern in an area at depth so actively degassing and characterized by very rapid morphological and geochemical variations. One of the most suitable physical parameters for gaining information about the subsurface structure is the electrical resistivity, which is highly sensitive to lithological variations, rock alterations, and fluid content (Unsworth & Rondenay, 2013).

Two main electrical conduction mechanisms characterize a fluid-saturated porous medium (Ghorbani et al., 2018; Rinaldi et al., 2011). The first is associated with the fluid flow inside the pores through electromigration of charges into the connected pore space. A second conduction mechanism occurs at the pore water-mineral interface in the electrical double layer caused by the migration of weakly adsorbed counterions (usually cations; Ghorbani et al., 2018). The electrical conductivity of porous rock can be expressed as a combination of these two contributions, namely, the surface electrical conductivity and the pore fluid electrical conductivity. Changes in these two quantities are mainly due to variations in the fluid filling the pores, considering that wet rocks usually have higher conductivities than dry rocks (Rinaldi et al., 2011 and references therein). Surface and pore fluid conductivities depend linearly on temperature (Revil et al., 1998; Roberts, 2002; Vaughan et al., 1992). Moreover, a dependence on the rock matrix permeability and pore fluid salinity is also observed (Jardani & Revil, 2009).

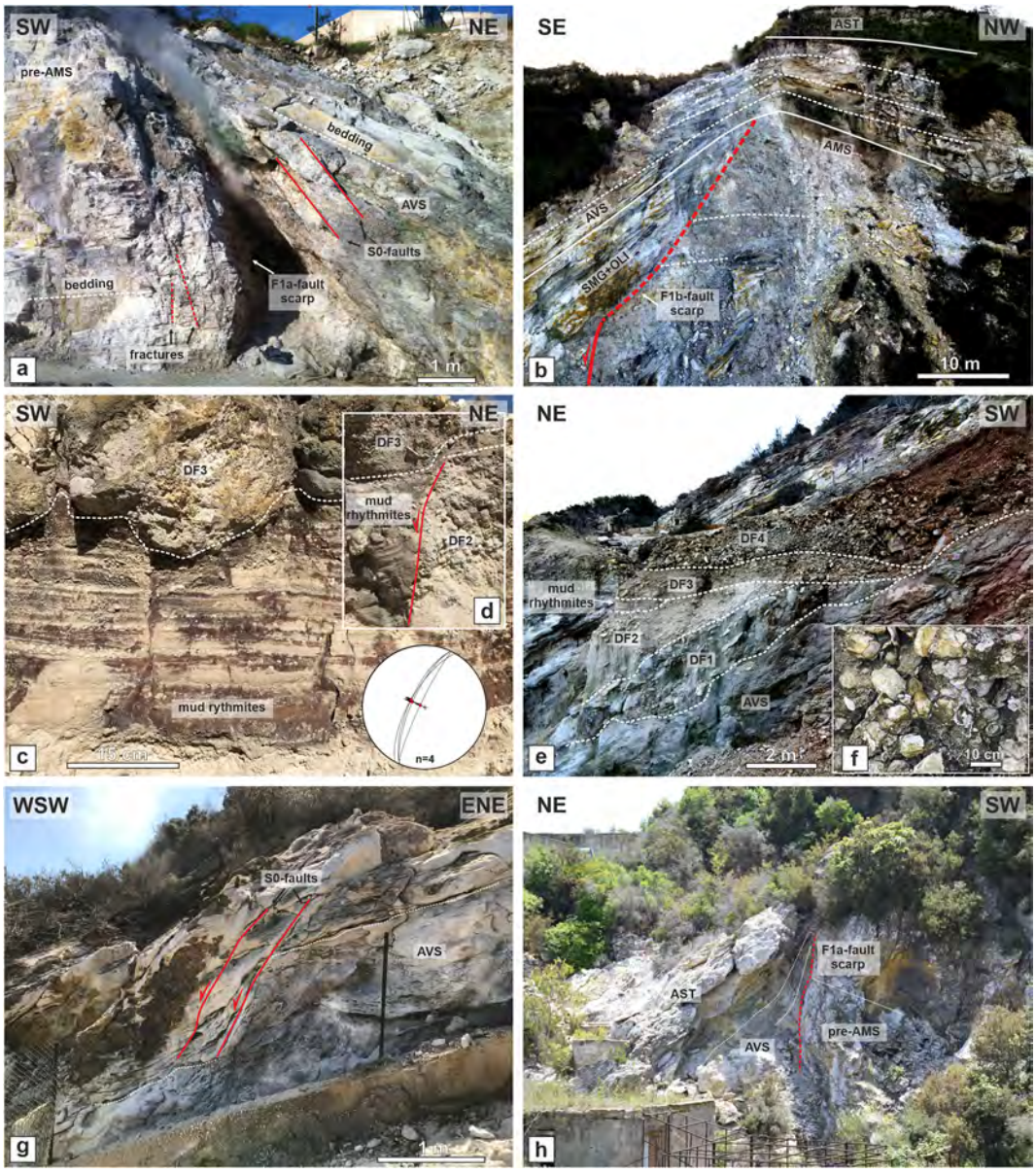

Figure 6. (a) F1a-fault scarp with pre-AMS in the footwall and covered by AVS deposits. (b) Panoramic view of the Pisciarelli slope showing the F1b-fault cutting AMS deposits and sealed by SMG, OLI, AVS and AST deposits. (c) Mud rhythmites embedded in debris flow deposits. (d) Particular of the mud sediments associated with a S2 synsedimentary normal fault. (e) View of the debris flow deposits and mud rhythmites (picture by UAV). (f) Hydrothermally cemented landslide debris. (g) Synsedimentary S0-faults in AVS deposits. (h) F1a-fault crosscutting the pre-AMS deposits and sealed by AVS and AST rocks.

Resistivity methods have been successfully applied to a wide variety of geological problems, including (1) hydrogeological and environmental problems (e.g., Kemna et al., 2002; Naudet et al., 2004), (2) the characterization of volcanoes and geothermal regions (Byrdina et al., 2014; Di Giuseppe & Troiano, 2019; Di Giuseppe, Troiano, Fedele, & Carlino, 2017; Di Giuseppe, Troiano, Di Vito, et al., 2017; Di Giuseppe, Troiano, Fedele, et al., 2015; Gresse et al., 2017; Tarchini et al., 2019; Troiano, Di Giuseppe, et al., 2014; Troiano, Isaia, et al., 2019; Troiano, Petrillo, et al., 2008), (3) the reconstruction of landslide structures (e.g., Lapenna et al., 2005; Lebourg et al., 2005), and (4) the localization and characterization of faults at shallow crustal levels (e.g., Caputo et al., 2003; Colella et al., 2004; Rizzo et al., 2004; Rizzo & Giampaolo, 2018; Suski et al., 2010).

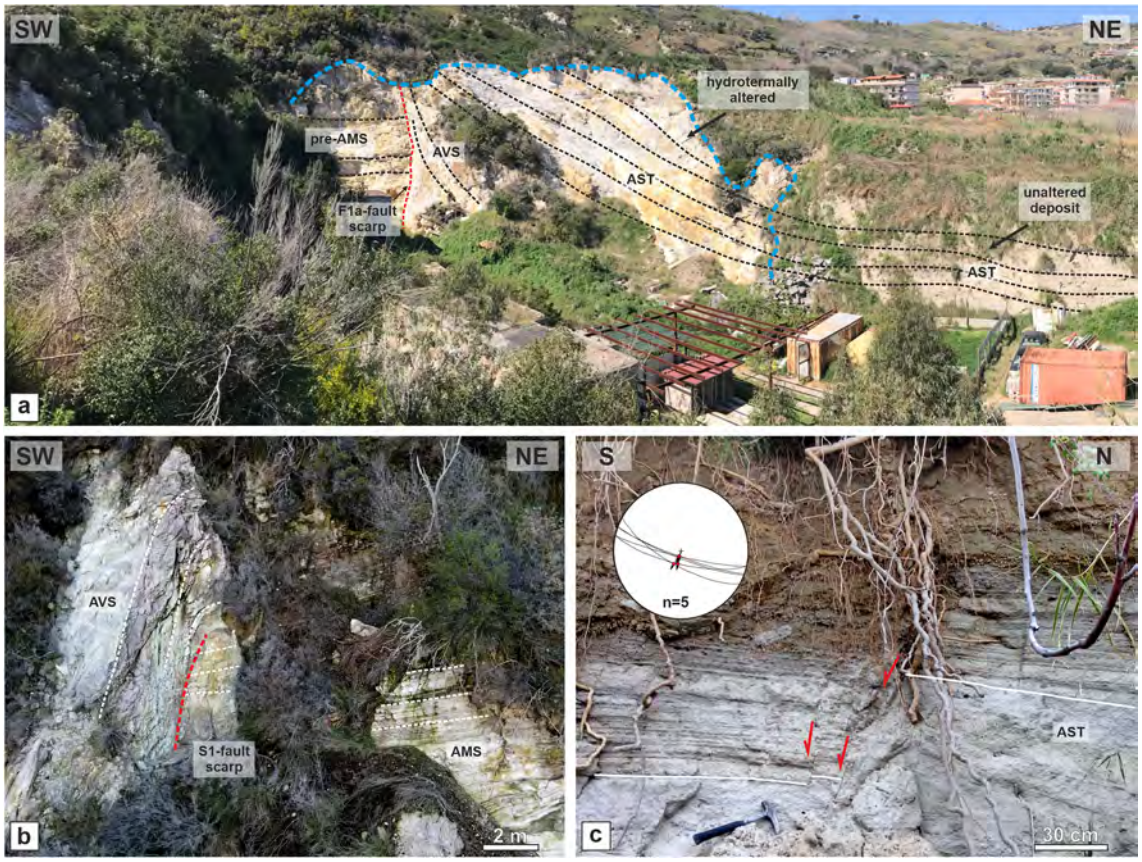

Figure 7. (a) Panoramic view of the NW side of the Pisciarelli area showing the F1a-fault cutting the pre-AMS deposits and sealed by AVS and AST rocks; note the heterogeneous hydrothermal alteration of the outcrop. (b) Particular of the contact between pre-AMS and AVS deposits. (c) S2-faults crosscutting the AST deposits (Via Antiniana).

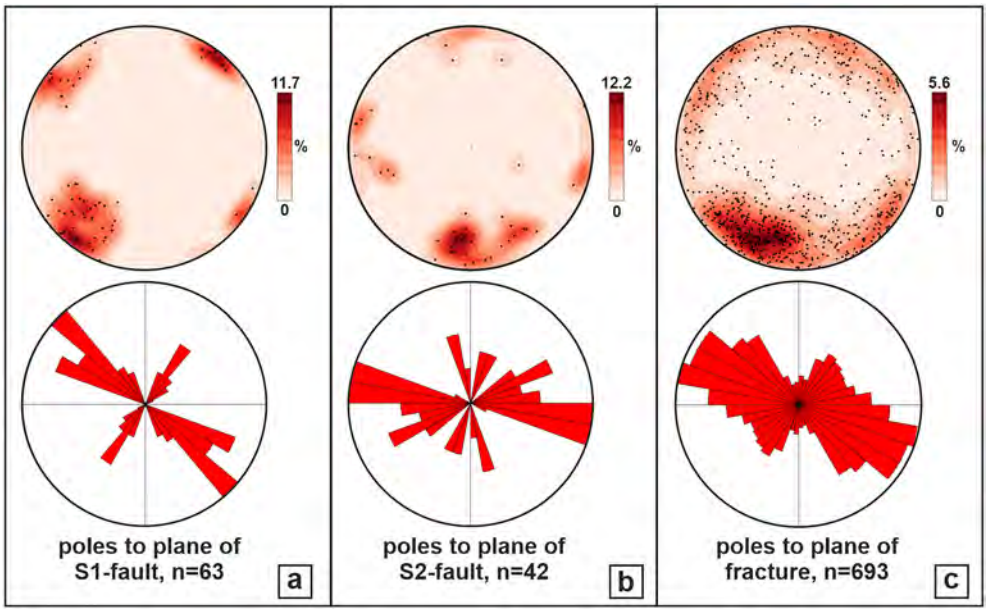

Figure 8. Stereographic projections (lower hemisphere, equiareal net) of the fault and fracture poles and corresponding rose diagrams.

In the geoelectrical method, a primary electric current is injected into the ground between two source electrodes. This current induces an electric field between two or more measurement voltage electrodes. Transferred resistances are then determined through Ohm's law, with the depth of investigation related to the distance between the source and voltage electrodes.

Modern geoelectrical imaging techniques are essentially based on the concept of remapping the same profile with a wide range of electrode spacings (Suski et al., 2010). The use of multipolar cables permits the contemporary deployment of a great number of electrodes in the field. The resulting multitude and partial redundancy of the current paths crossing the subsurface then lend themselves to tomographic imaging (e.g., Loke & Barker, 2004). The corresponding technique is called ERT.

In the present application, three ERT surveys (A-A′, B-B′, and C-C′ in Figure 5) were performed in 2019 to reconstruct the subsurface structure of the Pisciarelli site. An Iris Syscal Pro instrument was used as a multichannel resistivimeter. The same device was employed as a power source, producing a direct current with a maximum voltage and current of 800 V and 2 A, respectively. Several tens of electrodes were deployed in the field with uniform spacing. When the source current was injected between a couple of electrodes, the induced voltages were measured in correspondence with other electrode couples up to a distance of a fixed multiple of the spacing (realizing the so-called dipole-dipole configuration). In this way, a depth of approximately 100 m from the surface was investigated. Profiles A-A′ and B-B′ (crosscutting each other and trending NNW-SSE and W-E, respectively) correspond to 360 m long survey lines. The shorter C-C′ profile was 220 m in length and crossed the mud pool and main fumaroles in the Pisciarelli area in the W-E direction. For all these profiles, a 10 m electrode spacing was adopted. The ERT data, acquired in correspondence with each profile, were separately inverted, including topography, using ERTlab3D® commercial software. The inversion procedure was based on the smoothness-constrained least squares method inversion technique (LaBrecque et al., 1995). We used Occam's inverse algorithm (LaBrecque et al., 1995; Morelli & LaBrecque, 1996) to reconstruct the electrical resistivity image from the electric potential data. In the inversion routine, the subsurface is divided into rectangular regions of constant resistivity, and the optimization method adjusts the resistivity model to iteratively reduce the difference between the calculated and measured resistivity transfer values. Occam's inversion finds the smoothest possible model whose response best fits the measured data to an a priori chi-square statistic (Constable et al., 1987; de Groot-Hedlin & Constable, 1990). The model smoothness is enforced by minimizing the differences in the log resistivity of adjacent blocks. The conjugate-gradient method was employed to solve both the forward and inverse matrix systems, and a data-error reweighting scheme was implemented to suppress the effects of data outliers (Morelli & LaBrecque, 1996). The obtained root-mean-square (RMS) error is approximately 4, and the results are compatible with the volcanic environment (e.g., Vargemezis, 2014). To support the reliability of the images, it is common to look at S, the so-called sensitivity function, which takes into account the effects on the data by infinitesimal changes in the model resistivity. The sensitivity, which was estimated for all the tomograms, shows the degree to which a change in the resistivity of a section of the subsurface influences the potential measured by the array. The higher the value that the sensitivity function is, the greater the influence of the subsurface region on the measurement. In other words, this function tells us roughly how deep we can see with the performed array. The resistivity sections for each profile are reported in Figure 9a.

The tomograms show diffuse lateral and vertical heterogeneities within a resistivity range of approximately three orders of magnitude as an expression of a complex geological setting resulting from faulting, fracturing, and hydrothermal alteration processes that acted in the last 5.5 kyr. The sections show similar electrical patterns defined by a high resistivity zone (hundreds of Ω·m, indicated as a1 in Figure 9a) lying between two conductive layers (a few Ω·m), one deeper layer (labeled as b1 in Figure 9a) and one shallower layer (labeled b2 in Figure 9a). In particular, the Pisciarelli permanent mud pool and its main fumarole area, which are located in the intersection between the A-A′ and C-C′ profiles, are characterized by the largest conductive area b1.

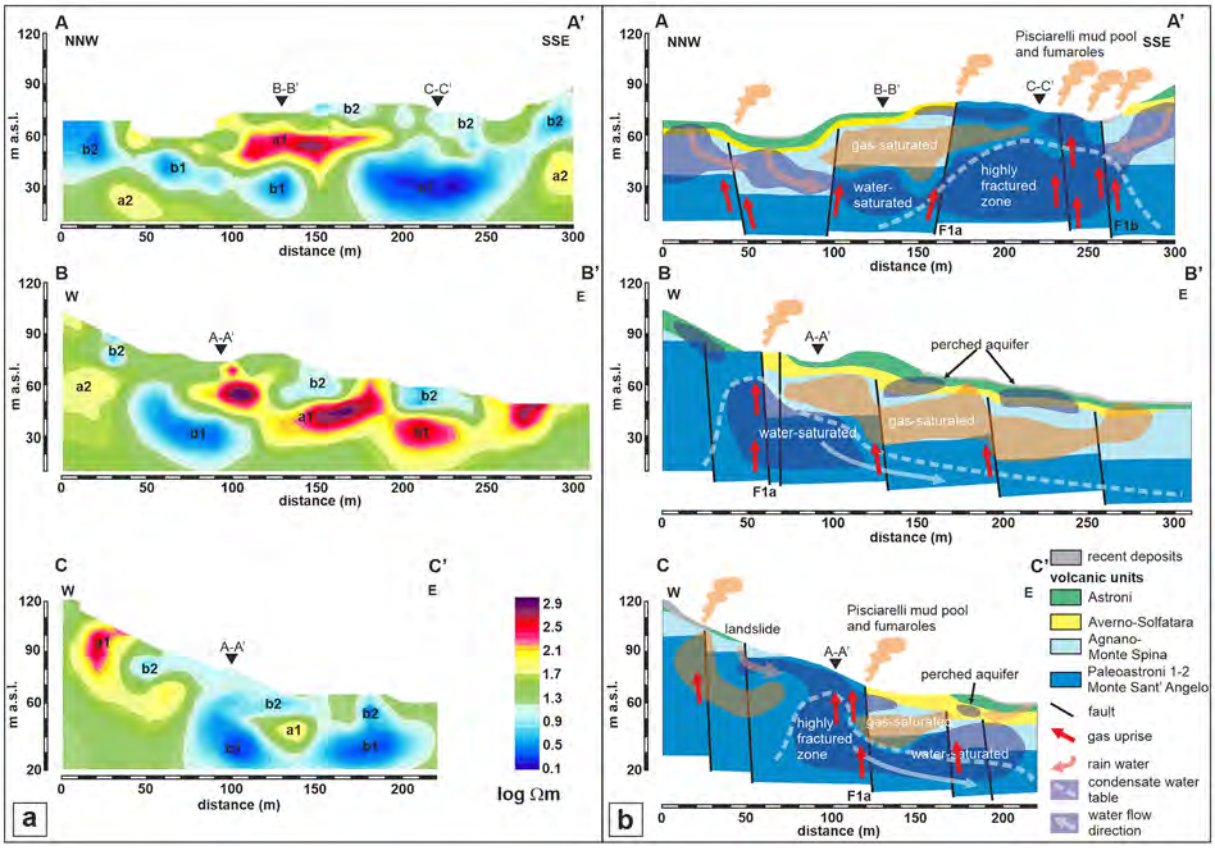

Figure 9. (a) ERT profiles. (b) Geological cross-sections (traces are shown in Figure 5).

5. Discussion

5.1. Mesoscale Exposed Structures

Geological and structural surveys have allowed us to draw a detailed geological map of the Pisciarelli area (Figure 5). Tectonic and volcanological features have been characterized by paying attention to their relationships with the intense hydrothermal emission distribution in the area. The geophysical survey has helped us to better constrain the main faults and to reconstruct their extension at depth. The structural survey has allowed us to recognize a local ductile-brittle deformation system (S0) and two main fault systems (S1 and S2). S0 structures show the characteristics of soft-sediment deformation and are associated with the deposition of volcanic products (Vitale & Isaia, 2014). Usually, their attitudes are conditioned by the preexisting morphology. In contrast, the S1 and S2 fault systems are widespread in the whole study area and are associated with the volcano-tectonic activity of the Campi Flegrei caldera (Vitale et al., 2019). The first system (S1), showing a NW-SE main direction and normal kinematics, affected the oldest exposed volcanoclastic succession (Pre-AMS and AMS deposits). Furthermore, S1 faults are covered by AVS deposits, indicating that they were active until ~4.28 ka, which was probably due to ground deformation preceding the Solfatara eruption, as observed elsewhere in the caldera (e.g., Vitale et al., 2019). Within the S1 system, two main faults, named F1a and F1b (Figures 5, 6a, 6b, 6h, 7a, and 7b), play a crucial role in intercepting and channeling the uprising hydrothermal fluids in the Pisciarelli area. In fact, the mud pool is located at their intersection; moreover, the main fumaroles occur along their surficial trace. Fault F1b hardly controls the morphological evolution of the head scarp receding along the western flank of the Solfatara volcano. The S2 fault system is characterized by smaller displacements (a few meters) and does not show a crucial role in controlling hydrothermal activity. Historical and ongoing events have also been accompanied by meters of ground deformation, which was likely associated with the reactivation of main faults, as already occurred during past deformation events (e.g., Di Luccio et al., 2015; La Rocca & Galluzzo, 2019; Vitale et al., 2019).

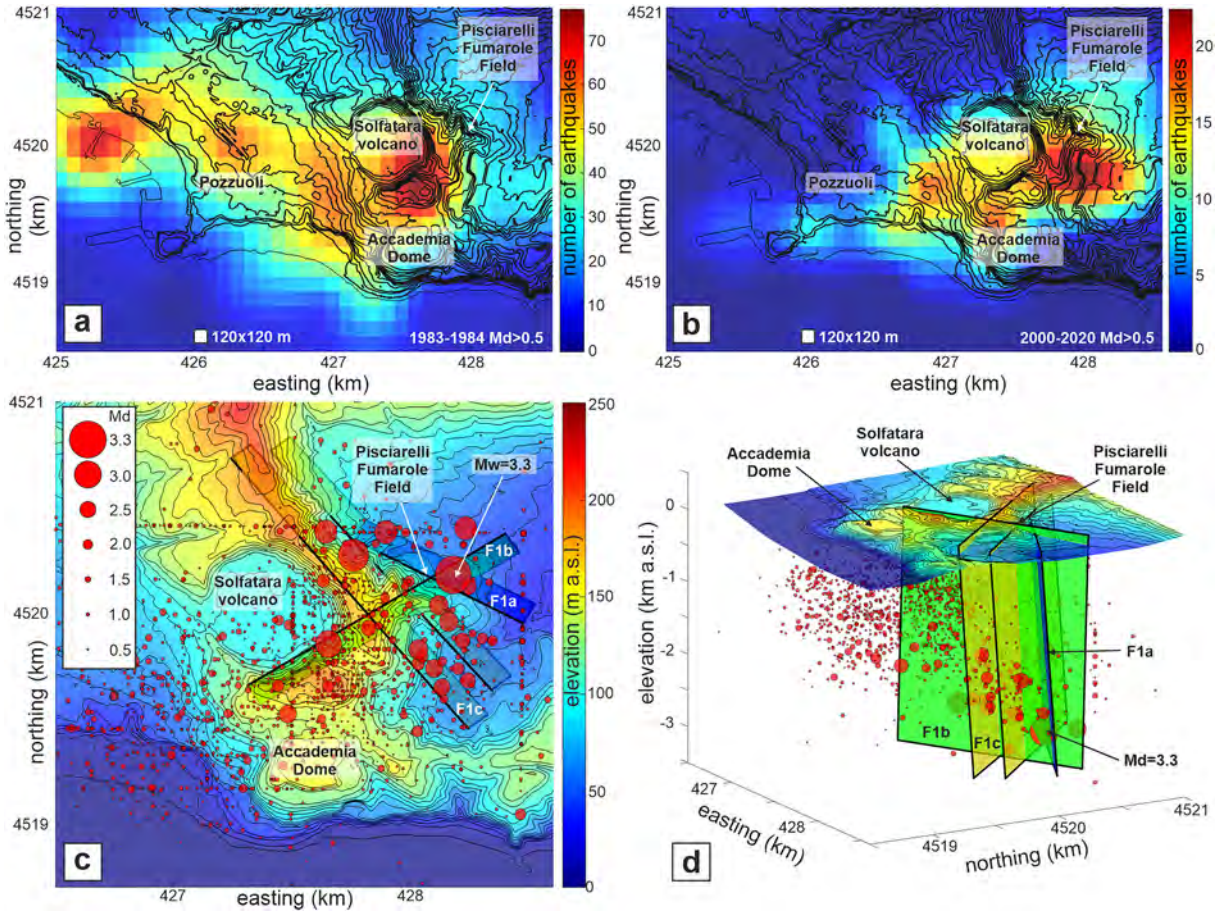

Figure 10. Earthquake number density (events/0.0144 km^2) maps in the Solfatara-Pisciarelli in: (a) 1983–1984 and (b) 2000–2020. Earthquake hypocenters in 2000–2020: (a) map view; (b) 3D view. Data refer to earthquakes with Md > 0.5. The E-W and N-S hypocenter alignments in (c) are artifacts related to the low-spatial resolution of the low-magnitude earthquakes.

Most of the high-frequency volcano-tectonic earthquakes (with Md > 0.5; OV-INGV, 2020b) of the 1983–1984 unrest event (Figure 10a), as well as the seismic events that occurred from 2000 to 2020 (Figure 10b), including the earthquake with the largest magnitude Md of 3.3 ± 0.3 (April 26, 2020; OV-INGV, 2020a), were localized in the Solfatara area. The relation between seismic hypocenters and surficial faults is not simple to reveal. Resistivity surveys performed in this work furnish structural information at shallow depths (100 m at depth). A deeper ERT survey of the central sector of the Campi Flegrei caldera reached a depth of 500 m (Troiano, Isaia, et al., 2019), indicating the same structural trends observed on the Earth's surface. The study also showed the shallow earthquakes (hypocenters <1 km b.s.l.), which are located between Solfatara and Pisciarelli, are confined eastward by a major NW-SE S1 fault (indicated as F1c in Figure 10c). The hypocentral depths of the largest earthquakes range between 2 and 3 km (for instance, the 2000–2020 seismic events with Md > 0.5 are shown in Figure 10d). Generally, the hypocenters cluster close to the S1 faults (Figure 10c). Considering that (1) the mapped faults are the principal pathways for the uprising magmatic fluids and (2) there is a strict geometric relation between the earthquake distribution and the surficial fault array, we suggest that the investigated faults are shallow expressions of deep-seated faults, as illustrated in Figure 10d. With this in mind, we envisage that the overpressurized fluids migrate upward, triggering fracturing, fault reactivation, and earthquakes. It is worth noting that by comparing the epicentral earthquake distributions in 1983–1984 (Figures 10a) and 2000–2020 (Figure 10b), the seismic activity moved from SW to NE, focusing in the area south of Pisciarelli. This is consistent with the fluid migration observed in the Solfatara-Pisciarelli area (Troiano, Isaia, et al., 2019; Young et al., 2020) and the sharp increase in hydrothermal activity in the Pisciarelli area starting in 2009 (OV-INGV Bulletin, 2020), including the opening of the main fumarole vent in 2013.

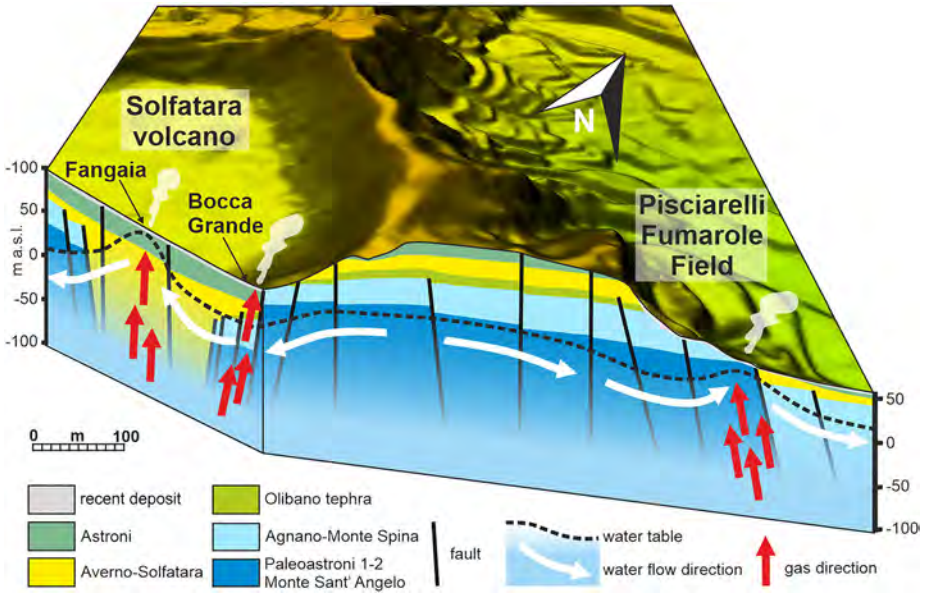

Figure 11. DEM and cross-section of the Solfatara-Pisciarelli area showing the interaction between uprising gases and water table.

5.2. ERT Interpretation: Interplay Between the Gas-Water System and Structures at Depth

The geological survey indicates that the stratigraphic setting of the study area is characterized by the superposition of pyroclastic deposits of the well-known eruptions of Epochs 3A and 3B. Generally, volcanic beds are subhorizontal or weakly dipping to the west and are crosscut by high-angle normal faults with displacements reaching a few tens of meters. Most deposits are composed of fine to coarse layers of pyroclastic materials. Hence, the variation in the resistivity values resulting from the ERT investigation is related to the water and/or gas content, which is mainly due to the rock permeability. The latter is strongly controlled by the fracturing intensity and eventual sealing processes related to hydrothermal activity (i.e., mineralization).

The ERT profiles highlight the alternation of more resistive (a1 in Figure 9a) and more conductive layers (b1 and b2 in Figure 9a), which are dislocated by subvertical structures that we interpret as normal faults. Some of these structures are well exposed, such as those shown in Figures 6 and 7 (F1a- and F1b-faults). Most of these normal faults lower the volcanic succession toward the Agnano Plain (located to the east). Combining data from the ERT profiles with information on the exposed geology, we draw three cross-sections (Figure 9b). The main F1a-fault, which is present in all cross-sections, corresponds to the principal NW-SE-striking fault dislocating the pre-AMS deposits in the Pisciarelli fumarole field (Figure 6a) and continues northwestward (Figures 7a and 7b). The other main fault F1b recognized in the area, represented in the A-A′ cross-section, corresponds to the NE-SW fault in Figure 6b. This normal fault, which we interpret as the prolongation of the fault passing through the Solfatara volcano, dislocates the pre-AVS succession, lowering the SE sector of the Pisciarelli area. According to field observations, the AVS deposits mantle the F1a-faults, crosscutting pre-AMS, AMS, and SMG deposits. In the A-A′ cross-section, the F1b-fault also occurs. Regarding the distribution of the more conductive and resistive bodies, we note that a large conductive zone is located under the Pisciarelli fumarole field (anomaly b1 in sections A-A′ and C-C′ of Figure 9a) and the old alum quarry and has a NW-SE trend. This feature suggests that the conductive volume follows the F1a-fault. We suggest that a high permeability characterizes this NW-SE-trending body due to intense fracturing and faulting. Hence, it allows gases to migrate upward. The piezometric surface, as reconstructed in the ERT profiles, is at least 20 meters higher in the Pisciarelli-old alum quarry sector than in the neighboring areas (Figure 11), where the water table depth is 30–50 m b.s.l. (Celico et al., 1992). According to Chiodini, Vandemeulebrouck, et al. (2015) and Tassi et al. (2013), these shallow fluids (b1) are mainly condensed water of upward migrating magmatic gases. This water/gas plume is similar to that reconstructed below the Fangaia mud pool within the Solfatara volcano (Byrdina et al., 2014; Isaia, Vitale, Di Giuseppe, et al., 2015). However, unlike this volcanic area, in the Pisciarelli fumarole field, condensed water does not accumulate

in a limited area, such as the Solfatara maar-diatreme volcano (see the reconstruction in Troiano, Isaia, et al., 2019). We hypothesize that this water entirely flows toward the Agnano Plain, which is the nearest depressed area acting as a water collection basin (Figure 11).

In summary, the ERT survey allowed us to reconstruct the geometry of the complex array of faults present in the Pisciarelli area and identify a NW-SE directed water plume associated with the condensation of uprising magmatic gases that are strictly linked to the main volcano-tectonic structures. Moreover, the F1a-fault and, in general, the NW-SE-trending structures of the S1 fault system act as a limit for the main resistive body (a1) that is well marked in the central sector of sections A-A′ and B-B′ (Figures 9a and 9b). This anomaly, which is approximately 100–150 m wide, is likely related to gas accumulation, as also suggested by larger-scale ERT images (Troiano, Isaia, et al., 2019). Finally, the ERT investigation strengthens the interpretation of considering these faults as the primary conduits for the uprising magmatic fluids. Hence, the self-sealing process mainly affects the host rocks, focusing on the fluid flow within the fault zones. This phenomenon can cause the pore pressure to increase, thereby decreasing the fault strength and triggering rock failures and earthquakes.

5.3. Volcanic Hazard Scenario

The investigated area of Pisciarelli includes a fumarole field that has dramatically changed in the last 15 years, with the formation of very powerful fumarolic vents and a very energetic mud pool, which continuously increases its surface area and the number of boiling points. The main fumarole vents experienced an escalation in temperature. Furthermore, an increase in the CO_2 flux has been measured in the whole emission area (Cardellini et al., 2017; Tamburello et al., 2019). Mud/gas explosions have been heard from locals, while small mud ejecta close to the pool have occurred and have recently been observed. On the other hand, a close relationship exists between the tremor associated with the fumarolic activity in the Pisciarelli area and the changes in the uplift rate, swarm seismicity, and hydrothermal activity (Giudicepietro et al., 2020). These phenomena and their ongoing variations are the most significant phenomena recorded in the caldera since the current unrest started in 2005. As discussed before, this sector of the caldera is also affected by the largest number of shallow high-frequency volcano-tectonic earthquakes (0.5–2.5 km b.s.l.) and seismic swarms recorded in recent years at the Campi Flegrei caldera (La Rocca & Galluzzo, 2019). Furthermore, the increase in hydrothermal and seismic activity led authorities to prohibit public access to this area. Our investigations clearly show that the fumaroles and mud pool of Pisciarelli localize along major faults, especially at their intersection (Figure 5). The impressive increase in fumarolic activity is likely due to increased gas flux from depth and a thermal change within the uppermost crust (Chiodini, Vandemeulebrouck, et al., 2015). These phenomena could favor fracturing and faulting reactivation and increase rock permeability. This feature is well highlighted at depth by the ERT image showing the formation of larger conductive bodies (anomaly b1 at approximately 270 m along profile A-A′ and 80 m along profile C-C′; Figure 9a) in the highly fractured zone close to the main faults (F1a and F1b in Figure 9b). These active structures facilitate the circulation of the fluids at shallow levels and/or the gas to escape as single fumarole vents. Any further enlargement of the emission area or increase in the fumarole activity (e.g., temperature and CO_2 flux) could be due to an increase in the gases from depth and/or rock fracturing. Both phenomena are strictly connected to the possible movement of magmatic fluids at depth. Particular settings, such as rocks characterized by several faults and related damage zones, could also lead to a sudden increase in heat flow and gas uprising, causing groundwater steaming and flashing that, in turn, may cause critical overpressure at shallow levels and trigger hydrothermal/phreatic explosions. Different phreatic eruptive events have occurred in the past at Campi Flegrei, which are mainly documented in the Solfatara area, including the initial phase of the Solfatara eruption, which destroyed a large lava dome complex and spread volcanic products in a wide area around the volcano (Isaia, Vitale, Di Giuseppe, et al., 2015). Lava dome intrusions and small phreatic/phreatomagmatic explosive events characterize this caldera sector and are favored by the activity of the fault systems described above (Figure 2a). These structures are common for both the Solfatara and Pisciarelli areas and are also the site of most of the seismicity that occurred recently at Campi Flegrei; therefore, they are structures capable of generating strong (reaching M 4.2, which occurred during the 1982–1984 unrest; De Natale & Zollo, 1986) shallow (<3–4 km) earthquakes. Hence, rock failure phenomena could occur in response to energetic seismic shock, with rock fracturing in the shallow hydrothermal system, and cause sudden fluid decompression, triggering explosive events (e.g., Gallagher et al., 2020; Kennedy et al., 2020).

However, further mechanisms may cause phreatic/hydrothermal eruptions. The present state of activity in the Pisciarelli area suggests an open system accompanied by continuous degassing and morphological variations in the mud pool, which only partly have a seasonal signature (Di Giuseppe & Troiano, 2019). The evolution of the degassing and fluid circulation activity may cause chemical alteration and mineral precipitation and hence favor the self-sealing of pores and fractures. For example, mineralogical analyses of samples collected in the Solfatara and Pisciarelli areas reveal intense surficial solfataric alteration made of amorphous silica and alunite (Mayer, Scheu, Montanaro, et al., 2016). The precipitation of alunite in pores and fractures due to fluid circulation leads to the formation of veins, as observed in the Pisciarelli area and other volcanoes (e.g., New Zealand; Gallagher et al., 2020; Kennedy et al., 2020). This process produces a decrease in the host rock permeability (e.g., Carlino et al., 2016) and, in turn, a pore pressure increase within the fault zones, which may trigger a hydrothermal explosion (Roman, LaFemina, et al., 2019).

Another mechanism that may cause a temporary obstruction of the fumarole vents and mud pool at Pisciarelli is the development of landslides. Field data show that a pile of mud rhythmites that is very similar to the sediment presently forming within the mud pool has been recognized approximately 14 m above it (Figures 6c–6e). This fossil mud pool deposit is embedded in debris flow deposits composed of large lithics and reworked scoriae produced during landslide events that were generated from the scarp close to the emission area. Locally, the debris is hydrothermally cemented (Figure 6f); furthermore, the whole sequence has been subsequently eroded. Finally, it is worth noting that the fossil mud pool deposit is associated with a synsedimentary fault (Figure 6d), suggesting that its formation was synchronous with a deformation stage that affected the area. Taking into account the latter features and other geological clues, such as (1) the changing morphology of the area, including the occurrence of unstable masses located uphill, (2) the chemical alteration of the rocks, and (3) the powerful hydrothermal activity mainly localized along the fault (F1b) passing for the head scarp, we suggest that a rapid closure of the main emission zones by landslide events could occur. The above-described phenomena have been tested worldwide in other hydrothermal systems (e.g., Rott et al., 2019), suggesting a possible trigger mechanism for an explosion that occurred in the past in the Pisciarelli area, as shown in the model of Figure 12. Figure 12a represents the starting state of the Pisciarelli fumarole field characterized by landslide deposits hosting fumaroles and a mud pool. A possible development scenario envisages a renewed landslide event producing a debris flow deposit, which forms an impermeable cap above the active fumarole area (Figure 12b). This seal increases the pressure within the shallow hydrothermal system, which could act as a trigger for an explosion capable of ejecting materials around the area (Figure 12c). The explosive event moved the main vents to a lower elevation, as observed currently (Figure 12d). We suggest that this scenario could again happen in the future, especially during energetic seismic events that are important trigger mechanisms for sliding phenomena (e.g., Keefer, 2002). However, horizontal migration of fluids through complex faults and fracture patterns and eventual leakage at the surface elsewhere cannot be ruled out as a consequence of the landslide covering the mud pool.

6. Conclusions

In this study, we have defined in detail the volcano-tectonic setting of the Pisciarelli area, representing basic knowledge crucial for understanding any possible evolution of volcanic activity in the area. The geological and volcanological survey has allowed us to provide a new geological map of the area and relative cross-sections. Morphological, stratigraphic, and structural analyses integrated with data from geoelectrical surveys suggest that the area is characterized by two main fault systems. The first (S1) affects the oldest part of the volcanoclastic succession, showing NW-SE and NW-SE main directions, normal kinematics, and displacement of tens of meters. The second fault system (S2) crosscuts all the previous structures and the youngest part of the volcanic succession. It is characterized by WNW-ESE and NNE-SSW main directions, normal kinematics, and a few meters of displacement.

The ERT survey, which consists of three profiles crosscutting the main fumaroles and mud pool, further sheds light on the deep structure of the Pisciarelli area. Resistivity anomalies outline the preferred fluid pathways, mainly located along two main S1 faults (named F1a and F1b) and at their intersection where highly fractured rocks occur. The reconstructed structural images show a complex hydrothermal system formed by a mix of upwelling gas, condensed water, and meteoric water. At depth, part of the recent

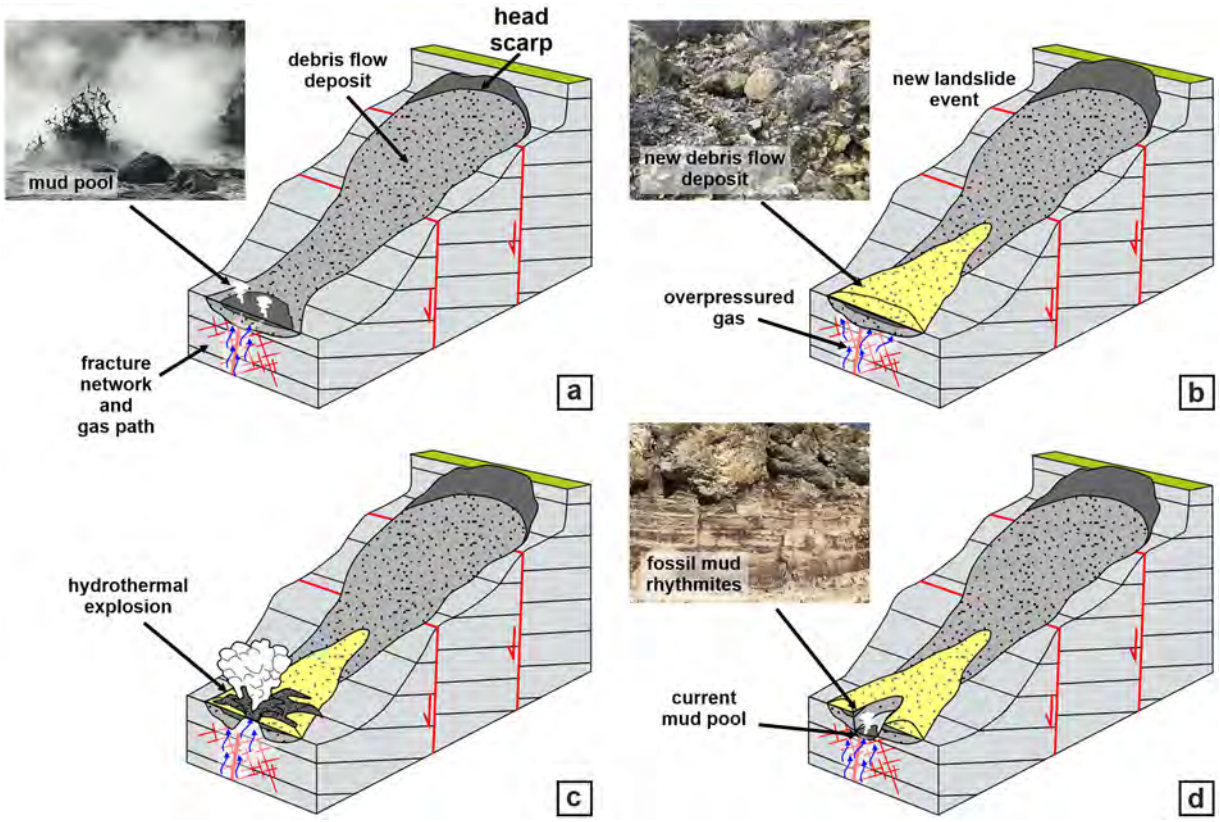

Figure 12. (a–d) Cartoon showing the hydrothermal and morphological evolution of the Pisciarelli area.

seismicity is distributed along the S1 faults, suggesting that, presently, these structures represent the main pathways for the upward migration of magmatic fluids within the Campi Flegrei system.

Field evidence also suggests that the main fumaroles and active mud pool could be obstructed by landslide deposits, as occurred in the past, causing critical overpressure in the shallow hydrothermal system and a possible explosion in the area. An increase in gas overpressure within the fault system could also be triggered by a decrease in the host rock permeability due to the self-sealing process. In contrast, an energetic seismic shock could cause large rock failure phenomena along the main faults, causing sudden fluid decompression in the shallow hydrothermal system and triggering explosive events.

The results of this multidisciplinary investigation provide new elements of knowledge on the active structures in this Campi Flegrei caldera sector, which are of fundamental importance for the forecast of future eruptive scenarios and have already experienced phreatic and hydrothermal eruptions. They further indicate how studies on the volcano-tectonic characterization of hydrothermal systems are necessary and crucial to shed light on their evolution, which recently, in several cases worldwide, rapidly evolved into eruptive phenomena causing human losses.

Although monitoring of the Pisciarelli area by the INGV-OV surveillance system is intensive, the proposed evolution scenarios indicate that further structural investigations at higher depths are necessary. In addition, highly detailed geophysical measurements reiterated in time or continuously are useful to detect any changes in the relationships between the faults and the hydrothermal fluid circulation.

Data Availability Statement

The data were collected in the framework of the INGV-DPC research agreement 2012–2021. This study does not necessarily represent the DPC official opinion and policies. The structural and electrical resistivity data used in this work are available in the following repository: R. Isaia, M. G. Di Giuseppe, J. Natale, F. D. A.

Tramparulo, A. Troiano, and S. Vitale (2021). Structural and electrical resistivity tomography data sets from "Volcano-tectonic setting of the Pisciarelli fumarole field, Campi Flegrei caldera, southern Italy: Insights into fluid circulation patterns and hazard scenarios", https://doi.org/10.6084/m9.figshare.14445582.

Acknowledgments
We thank the reviewers H. Geirsson and B. Christensen, the Associate Editor P. La Femina and the Editor J. Aitchinson for the useful and constructive suggestions that highly improved the paper. This work has benefited from funding provided by the Italian Presidenza del Consiglio dei Ministri - Dipartimento della Protezione Civile (DPC), agreement INGV-DPC.

References

Bellucci, F., Woo, J., Kilburn, C. R. J., & Rolandi, G. (2006). Ground deformation at Campi Flegrei, Italy: Implications for hazard assessment. *Geological Society, London, Special Publications*, *269*(1), 141–157. https://doi.org/10.1144/GSL.SP.2006.269.01.09

Bevilacqua, A., Flandoli, F., Neri, A., Isaia, R., & Vitale, S. (2016). Temporal models for the episodic volcanism of Campi Flegrei caldera (Italy) with uncertainty quantification. *Journal of Geophysical Research: Solid Earth*, *121*(11), 7821–7845. https://doi.org/10.1002/2016JB013171

Bevilacqua, A., Isaia, R., Neri, A., Vitale, S., Aspinall, W. P., Bisson, M., et al. (2015). Quantifying volcanic hazard at Campi Flegrei caldera (Italy) with uncertainty assessment: 1. Vent opening maps. *Journal of Geophysical Research: Solid Earth*, *120*(4), 2309–2329. https://doi.org/10.1002/2014JB011775

Bevilacqua, A., Neri, A., Bisson, M., Esposti Ongaro, T., Flandoli, F., Isaia, R., et al. (2017). The effects of vent location, event scale, and time forecasts on pyroclastic density current hazard maps at Campi Flegrei caldera (Italy). *Frontiers of Earth Science*, *5*, 72. https://doi.org/10.3389/feart.2017.00072

Bevilacqua, A., Neri, A., De Martino, P., Isaia, R., Novellino, A., Tramparulo, F. D. A., & Vitale, S. (2020). Radial interpolation of GPS and leveling data of ground deformation in a resurgent caldera: Application to Campi Flegrei (Italy). *Journal of Geodesy*, *94*, 24. https://doi.org/10.1007/s00190-020-01355-x

Byrdina, S., Vandemeulebrouck, J., Cardellini, C., Legaz, A., Camerlynck, C., Chiodini, G., et al. (2014). Relations between electrical resistivity, carbon dioxide flux, and self-potential in the shallow hydrothermal system of Solfatara (Phlegrean Fields, Italy). *Journal of Volcanology and Geothermal Research*, *283*, 172–182. https://doi.org/10.1016/j.jvolgeores.2014.07.010

Caputo, R., Piscitelli, S., Oliveto, A., Rizzo, E., & Lapenna, V. (2003). The use of electrical resistivity tomographies in active tectonics: Examples from the Tyrnavos Basin, Greece. *Journal of Geodynamics*, *36*(1–2), 19–35. https://doi.org/10.1016/s0264-3707(03)00036-x

Cardellini, C., Chiodini, G., Frondini, F., Avino, R., Bagnato, E., Caliro, S., et al. (2017). Monitoring diffuse volcanic degassing during volcanic unrests: The case of Campi Flegrei (Italy). *Scientific Reports*, *7*(1), 1–15. https://doi.org/10.1038/s41598-017-06941-2

Carlino, S., Troiano, A., Di Giuseppe, M. G., Tramelli, A., Troise, C., Somma, R., & De Natale, G. (2016). Exploitation of geothermal energy in active volcanic areas: A numerical modelling applied to high temperature Mofete geothermal field, at Campi Flegrei caldera (Southern Italy). *Renewable Energy*, *87*, 54–66. https://doi.org/10.1016/j.renene.2015.10.007

Celico, P., Dall'Aglio, M., Ghiara, M. R., Stanzione, D., & Brondi, M. (1992). Geochemical monitoring of the thermal fluids in the phlegraean fields from 1970 to 1990. *Bollettino della Societa Geologica Italiana*, *111*(3–4), 409–422.

Chiodini, G., Caliro, S., De Martino, P., Avino, R., & Gherardi, F. (2012). Early signals of new volcanic unrest at Campi Flegrei caldera? Insights from geochemical data and physical simulations. *Geology*, *40*(10), 943–946. https://doi.org/10.1130/G33251.1

Chiodini, G., Vandemeulebrouck, J., Caliro, S., D'Auria, L., De Martino, P., Mangiacapra, A., & Petrillo, Z. (2015). Evidence of thermal-driven processes triggering the 2005–2014 unrest at Campi Flegrei caldera. *Earth and Planetary Science Letters*, *414*, 58–67. https://doi.org/10.1016/j.epsl.2015.01.012

Christenson, B. W., Reyes, A. G., Young, R., Moebis, A., Sherburn, S., Cole-Baker, J., & Britten, K. (2010). Cyclic processes and factors leading to phreatic eruption events: Insights from the 25 September 2007 eruption through Ruapehu Crater Lake, New Zealand. *Journal of Volcanology and Geothermal Research*, *191*(1–2), 15–32. https://doi.org/10.1016/j.jvolgeores.2010.01.008

Christenson, B. W., White, S., Britten, K., & Scott, B. J. (2017). Hydrological evolution and chemical structure of a hyper-acidic spring-lake system on Whakaari/White Island, NZ. *Journal of Volcanology and Geothermal Research*, *346*, 180–211. https://doi.org/10.1016/j.jvolgeores.2017.06.017

Colella, A., Lapenna, V., & Rizzo, E. (2004). High-resolution imaging of the High Agri Valley Basin (Southern Italy) with electrical resistivity tomography. *Tectonophysics*, *386*(1–2), 29–40. https://doi.org/10.1016/j.tecto.2004.03.017

Constable, S. C., Parker, R. L., & Constable, C. G. (1987). Occam's inversion: A practical algorithm for generating smooth models from electromagnetic sounding data. *Geophysics*, *52*(3), 289–300. https://doi.org/10.1190/1.1442303

de Groot-Hedlin, C., & Constable, S. (1990). Occam's inversion to generate smooth, two-dimensional models from magnetotelluric data. *Geophysics*, *55*(12), 1613–1624. https://doi.org/10.1190/1.1442813

Deino, A. L., Orsi, G., de Vita, S., & Piochi, M. (2004). The age of the Neapolitan Yellow Tuff caldera-forming eruption (Campi Flegrei caldera – Italy) assessed by $^{40}Ar/^{39}Ar$ dating method. *Journal of Volcanology and Geothermal Research*, *133*, 157–170. https://doi.org/10.1016/S0377-0273(03)00396-2

Del Gaudio, C., Aquino, I., Ricciardi, G. P., Ricco, C., & Scandone, R. (2010). Unrest episodes at Campi Flegrei: A reconstruction of vertical ground movements during 1905–2009. *Journal of Volcanology and Geothermal Research*, *195*(1), 48–56. https://doi.org/10.1016/j.jvolgeores.2010.05.014

de Moor, J. M., Aiuppa, A., Pacheco, J., Avard, G., Kern, C., Liuzzo, M., et al. (2016). Short-period volcanic gas precursors to phreatic eruptions: Insights from Poás Volcano, Costa Rica. *Earth and Planetary Science Letters*, *442*, 218–227. https://doi.org/10.1016/j.epsl.2016.02.056

Dempsey, D. E., Cronin, S. J., Mei, S., & Kempa-Liehr, A. W. (2020). Automatic precursor recognition and real-time forecasting of sudden explosive volcanic eruptions at Whakaari, New Zealand. *Nature Communications*, *11*, 3562. https://doi.org/10.1038/s41467-020-17375-2

De Natale, G., & Zollo, A. (1986). Statistical analysis and clustering features of the Phlegraean Fields earthquake sequence (May 1983-May 1984). *Bulletin of the Seismological Society of America*, *76*(3), 801–814.

de Vita, S., Orsi, G., Civetta, L., Carandente, A., D'Antonio, M., Deino, A., et al. (1999). The Agnano–Monte Spina eruption (4100 years BP) in the restless Campi Flegrei caldera (Italy). *Journal of Volcanology and Geothermal Research*, *91*(2–4), 269–301. https://doi.org/10.1016/S0377-0273(99)00039-6

Di Giuseppe, M. G., & Troiano, A. (2019). Monitoring active fumaroles through time-lapse electrical resistivity tomograms: An application to the Pisciarelli fumarolic field (Campi Flegrei, Italy). *Journal of Volcanology and Geothermal Research*, *375*, 32–42. https://doi.org/10.1016/j.jvolgeores.2019.03.009

Di Giuseppe, M. G., Troiano, A., & Carlino, S. (2017). Magnetotelluric imaging of the resurgent caldera on the island of Ischia (southern Italy): Inferences for its structure and activity. *Bulletin of Volcanology*, *79*(12), 85. https://doi.org/10.1007/s00445-017-1170-4

Di Giuseppe, M. G., Troiano, A., Di Vito, M., Somma, R., & Matano, F. (2017). Definition of small-scale volcanic structures by Electrical Resistivity Tomography: The Trentaremi cone, an example from the Campi Flegrei Caldera (Italy). *Annals of Geophysics*, *60*(5), 0552. https://doi.org/10.4401/ag-7397

Di Giuseppe, M. G., Troiano, A., Fedele, A., Caputo, T., Patella, D., Troise, C., & De Natale, G. (2015). Electrical resistivity tomography imaging of the near-surface structure of the Solfatara Crater, Campi Flegrei (Naples, Italy). *Bulletin of Volcanology*, *77*(4), 27. https://doi.org/10.1007/s00445-015-0910-6

Di Luccio, F., Pino, N. A., Piscini, A., & Ventura, G. (2015). Significance of the 1982–2014 Campi Flegrei seismicity: Preexisting structures, hydrothermal processes, and hazard assessment. *Geophysical Research Letters*, *42*(18), 7498–7506. https://doi.org/10.1002/2015GL064962

Di Vito, M. A., Acocella, V., Aiello, G., Barra, D., Battaglia, M., Carandente, A., et al. (2016). Magma transfer at Campi Flegrei caldera (Italy) before the 1538 AD eruption. *Scientific Reports*, *6*, 32245. https://doi.org/10.1038/srep32245

Di Vito, M. A., Isaia, R., Orsi, G., Southon, J., de Vita, S., D'Antonio, M., et al. (1999). Volcanism and deformation in the past 12 ka at the Campi Flegrei caldera (Italy). *Journal of Volcanology and Geothermal Research*, *91*(2–4), 221–246. https://doi.org/10.1016/S0377-0273(99)00037-2

Di Vito, M. A., Lirer, L., Mastrolorenzo, G., & Rolandi, G. (1987). The 1538 Monte Nuovo eruption (Campi Flegrei, Italy). *Bulletin of Volcanology*, *49*(4), 608–615. https://doi.org/10.1007/BF01079966

Edwards, M. J., Kennedy, B. M., Jolly, A. D., Scheu, B., & Jousset, P. (2017). Evolution of a small hydrothermal eruption episode through a mud pool of varying depth and rheology, White Island, NZ. *Bulletin of Volcanology*, *79*(2), 16. https://doi.org/10.1007/s00445-017-1100-5

Gallagher, A., Montanaro, C., Cronin, S., Scott, B., Dingwell, D. B., & Scheu, B. (2020). Hydrothermal eruption dynamics reflecting vertical variations in host rock geology and geothermal alteration, Champagne Pool, Wai-o-tapu, New Zealand. *Bulletin of Volcanology*, *82*, 77. https://doi.org/10.1007/s00445-020-01414-3

Geirsson, H., Rodgers, M., LaFemina, P., Witter, M., Roman, D., Muñoz, A., et al. (2014). Multidisciplinary observations of the 2011 explosive eruption of Telica volcano, Nicaragua: Implications for the dynamics of low-explosivity ash eruptions. *Journal of Volcanology and Geothermal Research*, *271*, 55–69. https://doi.org/10.1016/j.jvolgeores.2013.11.009

Geshi, N., Iguchi, M., & Shinohara, H. (2016). Phreatomagmatic eruptions of 2014 and 2015 in Kuchinoerabujima Volcano triggered by a shallow intrusion of magma. *Journal of Natural Disaster Science*, *37*(2), 67–78. https://doi.org/10.2328/jnds.37.67

Ghorbani, A., Revil, A., Coperey, A., Soueid Ahmed, A., Roque, S., Heap, M. J., et al. (2018). Complex conductivity of volcanic rocks and the geophysical mapping of alteration in volcanoes. *Journal of Volcanology and Geothermal Research*, *357*, 106–127. https://doi.org/10.1016/j.jvolgeores.2018.04.014

Giaccio, B., Hajdas, I., Isaia, R., Deino, A., & Nomade, S. (2017). High-precision ^{14}C and $^{40}Ar/^{39}Ar$ dating of the Campanian Ignimbrite (Y-5) reconciles the time-scales of climatic-cultural processes at 40 ka. *Scientific Reports*, *7*, 45940. https://doi.org/10.1038/srep45940

Giudicepietro, F., Chiodini, G., Avino, R., Brandi, G., Caliro, S., De Cesare, W., et al. (2020). Tracking episodes of seismicity and gas transport in Campi Flegrei caldera through seismic, geophysical, and geochemical measurements. *Seismological Research Letters*, *92*(2A), 965–975. https://doi.org/10.1785/0220200223

Gresse, M., Vandemeulebrouck, J., Byrdina, S., Chiodini, G., Revil, A., Johnson, T. C., et al. (2017). Three-dimensional electrical resistivity tomography of the Solfatara Crater (Italy): Implication for the multiphase flow structure of the shallow hydrothermal system. *Journal of Geophysical Research: Solid Earth*, *122*(11), 8749–8768. https://doi.org/10.1002/2017JB014389

Guidoboni, E., & Ciuccarelli, C. (2011). The Campi Flegrei caldera: Historical revision and new data on seismic crises, bradyseisms, the Monte Nuovo eruption and ensuing earthquakes (twelfth century 1582 AD). *Bulletin of Volcanology*, *73*(6), 655–677. https://doi.org/10.1007/s00445-010-0430-3

Hanagan, C., La Femina, P. C., & Rodgers, M. (2020). Changes in crater morphology associated with volcanic activity at Telica volcano, Nicaragua. *Geochemistry, Geophysics, Geosystems*, *21*(7), e2019GC008889. https://doi.org/10.1029/2019GC008889

Harada, M., Doke, R., Mannen, K., Itadera, K., & Satomura, M. (2018). Temporal changes in inflation sources during the 2015 unrest and eruption of Hakone volcano, Japan. *Earth, Planets and Space*, *70*(1), 152. https://doi.org/10.1186/s40623-018-0923-4

Heap, M. J., Gravley, D. M., Kennedy, B. M., Gilg, H. A., Bertolett, E., & Barker, S. L. L. (2020). Quantifying the role of hydrothermal alteration in creating geothermal and epithermal mineral resources: The Ohakuri ignimbrite (Taupō Volcanic Zone, New Zealand). *Journal of Volcanology and Geothermal Research*, *390*, 106703. https://doi.org/10.1016/j.jvolgeores.2019.106703

Heap, M. J., Lavallée, Y., Petrakova, L., Baud, P., Reuschlé, T., Varley, N. R., & Dingwell, D. B. (2014). Microstructural controls on the physical and mechanical properties of edifice-forming andesites at Volcán de Colima, Mexico. *Journal of Geophysical Research: Solid Earth*, *119*(4), 2925–2963. https://doi.org/10.1002/2013JB010521

Hurst, T., Jolly, A. D., & Sherburn, S. (2014). Precursory characteristics of the seismicity before the 6 August 2012 eruption of Tongariro volcano, North Island, New Zealand. *Journal of Volcanology and Geothermal Research*, *286*, 294–302. https://doi.org/10.1016/j.jvolgeores.2014.03.004

Hurwitz, S., Clor, L. E., McCleskey, R. B., Nordstrom, D. K., Hunt, A. G., & Evans, W. C. (2016). Dissolved gases in hydrothermal (phreatic) and geyser eruptions at Yellowstone National Park, USA. *Geology*, *44*(3), 235–238. https://doi.org/10.1130/G37478.1

INGV. (2020). *Bollettini di sorveglianza dei vulcani campani*. Retrieved from http://www.ov.ingv.it/ov/it/bollettini.html

Isaia, R., D'Antonio, M., Dell'Erba, F., Di Vito, M., & Orsi, G. (2004). The Astroni volcano: The only example of closely spaced eruptions in the same vent area during the recent history of the Campi Flegrei caldera (Italy). *Journal of Volcanology and Geothermal Research*, *133*(1–4), 171–192. https://doi.org/10.1016/S0377-0273(03)00397-4

Isaia, R., Marianelli, P., & Sbrana, A. (2009). Caldera unrest prior to intense volcanism in Campi Flegrei (Italy) at 4.0 ka B.P.: Implications for caldera dynamics and future eruptive scenarios. *Geophysical Research Letters*, *36*(21), L21303. https://doi.org/10.1029/2009GL040513

Isaia, R., Vitale, S., Di Giuseppe, M. G., Iannuzzi, E., D'Assisi Tramparulo, F., & Troiano, A. (2015). Stratigraphy, structure, and volcano-tectonic evolution of Solfatara maar-diatreme (Campi Flegrei, Italy). *Geological Society of America Bulletin*, *127*(9–10), 1485–1504. https://doi.org/10.1130/B31183.1

Isaia, R., Vitale, S., Marturano, A., Aiello, G., Barra, D., Ciarcia, S., et al. (2019). High-resolution geological investigations to reconstruct the long-term ground movements in the last 15 kyr at Campi Flegrei caldera (southern Italy). *Journal of Volcanology and Geothermal Research*, *385*, 143–158. https://doi.org/10.1016/j.jvolgeores.2019.07.012

Jardani, A., & Revil, A. (2009). Stochastic joint inversion of temperature and self-potential data. *Geophysical Journal International*, *179*(1), 640–654. https://doi.org/10.1111/j.1365-246X.2009.04295.x

Jolly, A., Lokmer, I., Christenson, B., & Thun, J. (2018). Relating gas ascent to eruption triggering for the April 27, 2016, White Island (Whakaari), New Zealand eruption sequence. *Earth, Planets and Space*, *70*(1), 1–15. https://doi.org/10.1186/s40623-018-0948-8

Jolly, A. D., Jousset, P., Lyons, J. J., Carniel, R., Fournier, N., Fry, B., & Miller, C. (2014). Seismo-acoustic evidence for an avalanche driven phreatic eruption through a beheaded hydrothermal system: An example from the 2012 Tongariro eruption. *Journal of Volcanology and Geothermal Research*, *286*, 331–347. https://doi.org/10.1016/j.jvolgeores.2014.04.007

Keefer, D. K. (2002). Investigating landslides caused by earthquakes – A historical review. *Surveys in Geophysics*, *23*(6), 473–510. https://doi.org/10.1023/A:1021274710840

Kemna, A., Vanderborght, J., Kulessa, B., & Vereecken, H. (2002). Imaging and characterisation of subsurface solute transport using electrical resistivity tomography (ERT) and equivalent transport models. *Journal of Hydrology*, *267*(3–4), 125–146. https://doi.org/10.1016/s0022-1694(02)00145-2

Kennedy, B. M., Farquhar, A., Hilderman, R., Villeneuve, M. C., Heap, M. J., Mordensky, S., et al. (2020). Pressure controlled permeability in a conduit filled with fractured hydrothermal breccia reconstructed from ballistics from Whakaari (White Island), New Zealand. *Geosciences*, *10*(4), 138. https://doi.org/10.3390/geosciences10040138

Kilgour, G., Gates, S., Kennedy, B., Farquhar, A., McSporran, A., & Asher, C. (2019). Phreatic eruption dynamics derived from deposit analysis: A case study from a small, phreatic eruption from Whakāri/White Island, New Zealand. *Earth, Planets and Space*, *71*(1), 36. https://doi.org/10.1186/s40623-019-1008-8

Kobayashi, T., & Hatano, S. (1989). Genetic relation between phreatic explosions of the 4th volcanic period and fault movements of Midagahara fault on Tateyama volcano, central Honshu. *Bulletin of the Volcanological Society of Japan*, *34*(4), 348. https://doi.org/10.18940/kazanc.34.4348-2

LaBrecque, D. J., Morelli, G., Daily, B., Ramirez, A., & Lundegard, P. (1995). Occam's inversion of 3-D ERT data. In B. Spies (Ed.), *Three-dimensional electromagnetics* (pp. 575–590). SEG.

Lapenna, V., Lorenzo, P., Perrone, A., Piscitelli, S., Rizzo, E., & Sdao, F. (2005). 2D electrical resistivity imaging of some complex landslides in Lucanian Apennine chain, southern Italy. *Geophysics*, *70*(3), B11–B18. https://doi.org/10.1190/1.1926571

La Rocca, M., & Galluzzo, D. (2019). Focal mechanisms of recent seismicity at Campi Flegrei, Italy. *Journal of Volcanology and Geothermal Research*, *388*, 106687. https://doi.org/10.1016/j.jvolgeores.2019.106687

Lebourg, T., Binet, S., Tric, E., Jomard, H., & El Bedoui, S. (2005). Geophysical survey to estimate the 3D sliding surface and the 4D evolution of the water pressure on part of a deep seated landslide. *Terra Nova*, *17*(5), 399–406. https://doi.org/10.1111/j.1365-3121.2005.00623.x

Loke, M. H., & Barker, R. (2004). *RES2Dinv software*. Geotomo Software Company.

Mannen, K., Yukutake, Y., Kikugawa, G., Harada, M., Itadera, K., & Takenaka, J. (2018). Chronology of the 2015 eruption of Hakone volcano, Japan: Geological background, mechanism of volcanic unrest and disaster mitigation measures during the crisis. *Earth, Planets and Space*, *70*, 68. https://doi.org/10.1186/s40623-018-0844-2

Marturano, A., Isaia, R., Aiello, G., & Barra, D. (2018). Complex dome growth at Campi Flegrei caldera (Italy) in the last 15 ka. *Journal of Geophysical Research: Solid Earth*, *123*(9), 8180–8197. https://doi.org/10.1029/2018jb015672

Mayer, K., Scheu, B., Montanaro, C., Yilmaz, T. I., Isaia, R., Aßbichler, D., & Dingwell, D. B. (2016). Hydrothermal alteration of surficial rocks at Solfatara (Campi Flegrei): Petrophysical properties and implications for phreatic eruption processes. *Journal of Volcanology and Geothermal Research*, *320*, 128–143. https://doi.org/10.1016/j.jvolgeores.2016.04.020

Mayer, K., Scheu, B., Yilmaz, T. I., Montanaro, C., Albert Gilg, H., Rott, S., et al. (2017). Phreatic activity and hydrothermal alteration in the Valley of Desolation, Dominica, Lesser Antilles. *Bulletin of Volcanology*, *79*(12), 82. https://doi.org/10.1007/s00445-017-1166-0

Montanaro, C., Cronin, S., Scheu, B., Kennedy, B., & Scott, B. (2020). Complex crater fields formed by steam-driven eruptions: Lake Okaro, New Zealand. *GSA Bulletin*, *132*(9–10), 1914–1930. https://doi.org/10.1130/B35276.1

Montanaro, C., Mayer, K., Isaia, R., Gresse, M., Scheu, B., Yilmaz, T. I., et al. (2017). Hydrothermal activity and subsoil complexity: Implication for degassing processes at Solfatara crater, Campi Flegrei caldera. *Bulletin of Volcanology*, *79*(12), 83. https://doi.org/10.1007/s00445-017-1167-z

Montanaro, C., Scheu, B., Mayer, K., Orsi, G., Moretti, R., Isaia, R., & Dingwell, D. B. (2016). Experimental investigations on the explosivity of steam-driven eruptions: A case study of Solfatara volcano (Campi Flegrei). *Journal of Geophysical Research: Solid Earth*, *121*(11), 7996–8014. https://doi.org/10.1002/2016JB013273

Morelli, G., & LaBrecque, D. J. (1996). Advances in ERT inverse modelling. *European Journal of Environmental and Engineering Geophysics*, *1*(2), 171–186.

Morgan, L. A., Shanks, W. C., & Pierce, K. L. (2009). *Hydrothermal processes above the Yellowstone magma chamber: Large hydrothermal systems and large hydrothermal explosions*. Geological Society of America. Special Paper 459. https://doi.org/10.1130/2009.2459(01)

Natale, J., Ferranti, L., Marino, C., & Sacchi, M. (2020). Resurgent-dome faults in the offshore of the Campi Flegrei caldera (Pozzuoli Bay, Campania): Preliminary results from high-resolution seismic reflection profiles. *Bollettino di Geofisica Teorica ed Applicata*, *61*. https://doi.org/10.4430/bgta0315

Naudet, V., Revil, A., Rizzo, E., Bottero, J.-Y., & Bégassat, P. (2004). Groundwater redox conditions and conductivity in a contaminant plume from geoelectrical investigations. *Hydrology and Earth System Sciences*, *8*(1), 8–22. https://doi.org/10.5194/hess-8-8-2004

Ohba, T., Yaguchi, M., Nishino, K., Numanami, N., Daita, Y., Sukigara, C., et al. (2019). Time variations in the chemical and isotopic composition of fumarolic gases at Hakone volcano, Honshu Island, Japan, over the earthquake swarm and eruption in 2015, interpreted by magma sealing model. *Earth, Planets and Space*, *71*(1), 48. https://doi.org/10.1186/s40623-019-1027-5

Orsi, G., Di Vito, M. A., & Isaia, R. (2004). Volcanic hazard assessment at the restless Campi Flegrei caldera. *Bulletin of Volcanology*, *66*(6), 514–530. https://doi.org/10.1007/s00445-003-0336-4

OV-INGV (2020a). *Bollettini mensili dei vulcani della Campania*. Retrieved from https://www.ov.ingv.it/ov/it/bollettini.html

OV-INGV (2020b). *Databese sismologico dei vulcani della Campania*. Retrieved from https://sismolab.ov.ingv.it/sismo/index.php

Parascandola, A. (1947). *I fenomeni bradisismici del Serapeo di Pozzuoli*. Stabilmento tipografico G. Genovese.

Pistolesi, M., Isaia, R., Marianelli, P., Bertagnini, A., Fourmentraux, C., Albert, P. G., et al. (2016). Simultaneous eruptions from multiple vents at Campi Flegrei (Italy) highlight new eruption processes at calderas. *Geology*, *44*(6), 487–490. https://doi.org/10.1130/G37870.1

Revil, A., Cathles, L. M., III, Losh, S., & Nunn, J. A. (1998). Electrical conductivity in shaly sands with geophysical applications. *Journal of Geophysical Research*, *103*(B10), 23925–23936. https://doi.org/10.1029/98jb02125

Rinaldi, A. P., Todesco, M., Vandemeulebrouck, J., Revil, A., & Bonafede, M. (2011). Electrical conductivity, ground displacement, gravity changes, and gas flow at Solfatara crater (Campi Flegrei caldera, Italy): Results from numerical modeling. *Journal of Volcanology and Geothermal Research*, *207*(3–4), 93–105. https://doi.org/10.1016/j.jvolgeores.2011.07.008

Rivalta, E., Corbi, F., Passarelli, L., Acocella, V., Davis, T., & Di Vito, M. A. (2019). Stress inversions to forecast magma pathways and eruptive vent location. *Science Advances*, *5*(7), eaau9784. https://doi.org/10.1126/sciadv.aau9784

Rizzo, E., Colella, A., Lapenna, V., & Piscitelli, S. (2004). High-resolution images of the fault-controlled High Agri Valley basin (Southern Italy) with deep and shallow electrical resistivity tomographies. *Physics and Chemistry of the Earth, Parts A/B/C*, *29*(4–9), 321–327. https://doi.org/10.1016/j.pce.2003.12.002

Rizzo, E., & Giampaolo, V. (2018). New deep electrical resistivity tomography in the High Agri Valley basin (Basilicata, Southern Italy). *Geomatics, Natural Hazards and Risk*, *10*(1), 197–218. https://doi.org/10.1080/19475705.2018.1520150

Roberts, J. J. (2002). Electrical properties of microporous rock as a function of saturation and temperature. *Journal of Applied Physics*, *91*(3), 1687–1694. https://doi.org/10.1063/1.1430544

Roman, D. C., LaFemina, P. C., Bussard, R., Stephens, K., Wauthier, C., Higgins, M., et al. (2019). Mechanisms of unrest and eruption at persistently restless volcanoes: Insights from the 2015 eruption of Telica Volcano, Nicaragua. *Geochemistry, Geophysics, Geosystems*, *20*(8), 4162–4183. https://doi.org/10.1029/2019GC008450

Roman, D. C., Rodgers, M., Geirsson, H., LaFemina, P. C., & Tenorio, V. (2016). Assessing the likelihood and magnitude of volcanic explosions based on seismic quiescence. *Earth and Planetary Science Letters*, *450*, 20–28. https://doi.org/10.1016/j.epsl.2016.06.020

Rott, S., Scheu, B., Montanaro, C., Mayer, K., Joseph, E. P., & Dingwell, D. B. (2019). Hydrothermal eruptions at unstable crater lakes: Insights from the Boiling Lake, Dominica, Lesser Antilles. *Journal of Volcanology and Geothermal Research*, *381*, 101–118. https://doi.org/10.1016/j.jvolgeores.2019.05.020

Salvage, R. O., Avard, G., De Moor, J. M., Pacheco, J. F., Brenes Marin, J., Cascante, M., et al. (2018). Renewed Explosive Phreatomagmatic Activity at Poás Volcano, Costa Rica in April 2017. *Frontiers of Earth Science*, *6*, 160. https://doi.org/10.3389/feart.2018.00160

Seki, K., Kanda, W., Ogawa, Y., Tanbo, T., Kobayashi, T., Hino, Y., & Hase, H. (2015). Imaging the hydrothermal system beneath the Jigokudani valley, Tateyama volcano, Japan: Implications for structures controlling repeated phreatic eruptions from an audio-frequency magnetotelluric survey. *Earth, Planets and Space*, *67*(1), 6–9. https://doi.org/10.1186/s40623-014-0169-8

Selva, J., Orsi, G., Di Vito, M. A., Marzocchi, W., & Sandri, L. (2012). Probability hazard map for future vent opening at the Campi Flegrei caldera, Italy. *Bulletin of Volcanology*, *74*(2), 497–510. https://doi.org/10.1007/s00445-011-0528-2

Smith, V. C., Isaia, R., & Pearce, N. J. G. (2011). Tephrostratigraphy and glass compositions of post-15 kyr Campi Flegrei eruptions: Implications for eruption history and chronostratigraphic markers. *Quaternary Science Reviews*, *30*(25–26), 3638–3660. https://doi.org/10.1016/j.quascirev.2011.07.012

Stix, J., & de Moor, J. M. (2018). Understanding and forecasting phreatic eruptions driven by magmatic degassing. *Earth, Planets and Space*, *70*(1), 83. https://doi.org/10.1186/s40623-018-0855-z

Suski, B., Brocard, G., Authemayou, C., Muralles, B. C., Teyssier, C., & Holliger, K. (2010). Localization and characterization of an active fault in an urbanized area in central Guatemala by means of geoelectrical imaging. *Tectonophysics*, *480*(1–4), 88–98. https://doi.org/10.1016/j.tecto.2009.09.028

Tajima, Y., Nakada, S., Maeno, F., Huruzono, T., Takahashi, M., Inamura, A., et al. (2020). Shallow magmatic hydrothermal eruption in April 2018 on Ebinokogen Ioyama volcano in Kirishima volcano group, Kyushu, Japan. *Geosciences*, *10*(5), 183. https://doi.org/10.3390/geosciences10050183

Tamburello, G., Caliro, S., Chiodini, G., De Martino, P., Avino, R., Minopoli, C., et al. (2019). Escalating CO_2 degassing at the Pisciarelli fumarolic system, and implications for the ongoing Campi Flegrei unrest. *Journal of Volcanology and Geothermal Research*, *384*, 151–157. https://doi.org/10.1016/j.jvolgeores.2019.07.005

Tarchini, L., Ranaldi, M., Carapezza, M., Di Giuseppe, M., Isaia, R., Lucchetti, C., et al. (2019). Multidisciplinary studies of diffuse soil CO_2 flux, gas permeability, self-potential, soil temperature highlight the structural architecture of Fondi di Baia craters (Campi Flegrei caldera, Italy). *Annals of Geophysics*, *61*. https://doi.org/10.4401/ag-7683

Tassi, F., Nisi, B., Cardellini, C., Capecchiacci, F., Donnini, M., Vaselli, O., et al. (2013). Diffuse soil emission of hydrothermal gases (CO_2, CH_4, and C_6H_6) at Solfatara crater (Campi Flegrei, southern Italy). *Applied Geochemistry*, *35*, 142–153. https://doi.org/10.1016/j.apgeochem.2013.03.020

Troiano, A., Di Giuseppe, M. G., Patella, D., Troise, C., & De Natale, G. (2014). Electromagnetic outline of the Solfatara-Pisciarelli hydrothermal system, Campi Flegrei (southern Italy). *Journal of Volcanology and Geothermal Research*, *277*, 9–21. https://doi.org/10.1016/j.jvolgeores.2014.03.005

Troiano, A., Isaia, R., Di Giuseppe, M. G., Tramparulo, F. D. A., & Vitale, S. (2019). Deep Electrical Resistivity Tomography for a 3D picture of the most active sector of Campi Flegrei caldera. *Scientific Reports*, *9*, 15124. https://doi.org/10.1038/s41598-019-51568-0

Troiano, A., Petrillo, Z., Di Giuseppe, M. G., Balasco, M., Diaferia, I., Di Fiore, B., et al. (2008). About the shallow resistivity structure of Vesuvius volcano. *Annals of Geophysics*, *51*, 181–189.

Unsworth, M., & Rondenay, S. (2013). Mapping the distribution of fluids in the crust and lithospheric mantle utilizing geophysical methods. In *Lecture Notes in Earth System Sciences*. Springer. https://doi.org/10.1007/978-3-642-28394-9.13

Vargemezis, G. (2014). 3D geoelectrical model of geothermal spring mechanism derived from VLF measurements: A case study from Aggistro (Northern Greece). *Geothermics*, *51*, 1–8. https://doi.org/10.1016/j.geothermics.2013.09.001

Vaughan, G. B. M., Heiney, P. A., McCauley, J. P., Jr., & Smith, A. B., III (1992). Conductivity and structure of a liquid-crystalline organic conductor. *Physical Review B: Condensed Matter*, *46*(5), 2787–2791. https://doi.org/10.1103/physrevb.46.2787

Vilardo, G., Isaia, R., Ventura, G., De Martino, P., & Terranova, C. (2010). InSAR Permanent Scatterer analysis reveals fault re-activation during inflation and deflation episodes at Campi Flegrei caldera. *Remote Sensing of Environment*, *114*(10), 2373–2383. https://doi.org/10.1016/j.rse.2010.05.014

Vitale, S., & Ciarcia, S. (2013). Tectono-stratigraphic and kinematic evolution of the southern Apennines/Calabria-Peloritani Terrane system (Italy). *Tectonophysics*, *583*, 164–182. https://doi.org/10.1016/j.tecto.2012.11.004

Vitale, S., & Isaia, R. (2014). Fractures and faults in volcanic rocks (Campi Flegrei, southern Italy): Insight into volcano-tectonic processes. *International Journal of Earth Sciences*, *103*(3), 801–819. https://doi.org/10.1007/s00531-013-0979-0

Vitale, S., Isaia, R., Ciarcia, S., Di Giuseppe, M. G., Iannuzzi, E., Prinzi, E. P., et al. (2019). Seismically induced soft-sediment deformation phenomena during the volcano-tectonic activity of Campi Flegrei caldera (southern Italy) in the last 15 kyr. *Tectonics*, *38*(6), 1999–2018. https://doi.org/10.1029/2018TC005267

Young, N., Isaia, R., & Gottsmann, J. (2020). Gravimetric constraints on the hydrothermal system of the Campi Flegrei caldera. *Journal of Geophysical Research: Solid Earth*, *125*(7), e2019JB019231. https://doi.org/10.1029/2019jb019231